1   In preparation for Rapid Communications in Mass Spectrometry
2   **pyisotopomer: A Python package for obtaining intramolecular isotope ratio differences**
3   **from mass spectrometric analysis of nitrous oxide isotopocules**

4   Colette L. Kelly,[1*] Cara Manning,[2] Claudia Frey,[3] Jan Kaiser,[4] Noah Gluschankoff,[1] and Karen
5   L. Casciotti

6   1. Stanford University, Department of Earth System Science, Stanford, CA 94305, USA
7   2. University of Connecticut, Department of Marine Sciences, Groton, CT, 06340, USA
8   3. Department of Environmental Science, University of Basel, Basel, Switzerland.
9   4. University of East Anglia, Centre for Ocean and Atmospheric Sciences, School of
10   Environmental Sciences, Norwich, NR4 7TJ, UK
11
12   *** Correspondence to:** Colette L. Kelly (email: clkelly@stanford.edu; phone: 802-595-3647;
13   address: 473 Via Ortega Room 140, Stanford, CA 94305).

14
15   **Keywords:** Nitrous oxide, isotopomers, isotopocules, scrambling, Python
16
17   **Abstract**
18

19   **RATIONALE** Obtaining nitrous oxide isotopocule measurements with isotope ratio mass
20   spectrometry (IRMS) involves analyzing the ion current ratios of the nitrous oxide parent ion
21   (N_2O^+) as well as those of the NO^+ fragment ion. The data analysis requires correcting for
22   "scrambling" in the ion source, whereby the NO^+ fragment ion obtains the outer N atom from the
23   N_2O molecule. While descriptions exist for this correction, and interlaboratory intercalibration
24   efforts have been made, there has yet to be published a package of code for implementing
25   isotopomer calibrations.
26
27   **METHODS** We developed a user-friendly Python package (pyisotopomer) to determine two
28   coefficients (γ and κ) that describe scrambling in the IRMS ion source, and then to use this
29   calibration to obtain intramolecular isotope deltas in N_2O samples.
30
31   **RESULTS** With two appropriate reference materials, γ and κ can be determined robustly and
32   accurately for a given IRMS. An additional third reference material is needed to define the zero-
33   point of the delta scale. We show that IRMS scrambling behavior can vary with time,
34   necessitating regular calibrations. Finally, we present an intercalibration between two IRMS
35   laboratories, using pyisotopomer to calculate γ and κ, and to obtain intramolecular N_2O isotope
36   deltas in lake water unknowns.
37
38   **CONCLUSIONS** Given these considerations, we discuss how to use pyisotopomer to obtain
39   high-quality N_2O isotopocule data from IRMS systems, including the use of appropriate
40   reference materials and frequency of calibration.

1. Introduction

Nitrous oxide (N$_2$O) is a potent greenhouse gas, with a global warming potential 265 times that of carbon dioxide over a 100 year time horizon[1,2]. N$_2$O is also likely to be the most emitted ozone depletion agent in the 21st century, due to production of NO radicals in the stratosphere that interact destructively with ozone[3–6]. Historically, the bulk stable isotopes of nitrogen and oxygen in N$_2$O have been used to quantify its microbial cycling in soils[7,8] and in the ocean[9–12], its destruction by photolysis and O(^{1}D), and its cycling in the atmosphere[13,14]. This approach often fails at disentangling different N$_2$O production and consumption mechanisms, because the bulk nitrogen and oxygen isotope ratios of N$_2$O depend on the isotopic composition of the substrate, as well as the isotope effects of production and consumption processes[12]. Furthermore, in the context of microbial N$_2$O cycling in soils and the ocean, bacterial nitrification and denitrification produce N$_2$O with similar bulk $\delta(^{15}N)$[1] values, preventing partitioning between these processes on the basis of bulk $\delta(^{15}N)$ alone[15,16].

The site-specific nitrogen isotope ratios of N$_2$O provide a more nuanced constraint on the biogeochemical cycling of N$_2$O than its bulk composition alone. N$_2$O isotopomers have been used extensively to quantify its biogeochemical cycling in soils[17–20], the atmosphere[14,21–23], and the ocean[24–34]. The individual isotopic compositions of each nitrogen atom were first measured by Friedman and Bigeleisen, who quantified the yields of isotopomers $^{14}N^{15}N^{16}O$ and $^{15}N^{14}N^{16}O$ from enriched ammonium nitrate by measuring the NO$^+$ fragment ion signal in an isotope ratio mass spectrometer (IRMS)[35]. 50 years later, these N$_2$O isotopomers were quantified at natural abundance from the N$_2$O$^+$ species with mass numbers 44, 45, and 46 and the mass 30 and 31 NO$^+$ fragment ion[36,37]. The central nitrogen atom in the N$_2$O molecule has been designated with locants α, μ, or 2; the terminal atom, with locants β, τ, or 1[38,39]. Here, we use the definitions from Toyoda and Yoshida (1999) for the site-specific isotope number (N) ratios of the central (α) nitrogen atom and terminal (β) nitrogen atom[36]:

$$^{15}R^\alpha = \frac{N(^{14}N^{15}NO)}{N(^{14}N^{14}NO)} \tag{1}$$

$$^{15}R^\beta = \frac{N(^{15}N^{14}NO)}{N(^{14}N^{14}NO)} \tag{2}$$

The N$_2$O isotopomer measurement was initially performed with two sequential measurements of the same sample on an isotope ratio mass spectrometer, one at m/z 44, 45, and 46, and the other at m/z 30 and 31[36]. Use of dedicated cup-configurations on lower-dispersion IRMS instruments allowed simultaneous analysis of all five masses together[40].

The slight difference in absorption cross sections between the isotopocules of N$_2$O result in different isotopic fractionations during photolysis and photo-oxidation in the stratosphere[41], making the isotopomers of N$_2$O a powerful tool for understanding its atmospheric cycling[21,42–45]. Likewise, N$_2$O site preference, defined as $\delta(^{15}N^{sp}) = \delta(^{15}N^\alpha) - \delta(^{15}N^\beta)$, was shown in microbial culture experiments to be largely a function of reaction mechanism, independent of source composition[24,46–50]. This allowed for the differentiation between N$_2$O from bacterial nitrification ($\delta(^{15}N^{sp}) \approx 28\text{-}38$ ‰) and denitrification ($\delta(^{15}N^{sp}) \approx 0$)[24,46–50], although more studies are needed to better constrain the SPs for diverse fungal, bacterial, and archaeal strains in both terrestrial and

---

[1] We write δ values with parentheses, e.g., $\delta(^{15}N)$, because δ is the quantity symbol and "^{15}N" is the label. See SI Brochure: https://www.bipm.org/en/publications/si-brochure/

80　marine environments[49,51]. During N₂O consumption, $\delta(^{15}N^\alpha)$ and $\delta(^{18}O)$ were shown in microbial
81　culture[52] and soil mesocosm[19] experiments to exhibit a characteristic relationship, allowing
82　subsequent studies to use this relationship to distinguish between oxidative and reductive
83　regimes of N₂O cycling[30,33].
84　　　　Site-specific nitrogen isotope ratio measurements based on mass spectrometry need to be
85　corrected for a phenomenon called "scrambling," whereby the NO⁺ fragment ion contains the
86　terminal N atom, rather than the central N attached to the O atom (as in the original molecule). A
87　number of approaches have been taken to calibrate an IRMS system for this effect: 1) the use of
88　a single "rearrangement factor" to describe scrambling[36,53], 2) the use of nine coefficients to
89　describe the different fragmentation behaviors of the different isotopocules of N₂O[54], and finally
90　3) the use of two coefficients to describe scrambling in the ion source[50]. While descriptions exist
91　for each of these approaches, and interlaboratory intercalibration efforts have been made[55,56],
92　there has yet to be published a package of code for implementing any of the above isotopomer
93　calibrations.
94　　　　We developed a Python software package ("pyisotopomer") that implements the two-
95　coefficient approach described by Frame and Casciotti[32] to calibrate an IRMS for scrambling and
96　use that calibration to obtain high-quality N₂O isotopocule data. This software solves a set of
97　equations, either analytically or with an optimization routine, to quantify the scrambling behavior
98　of an IRMS. To quantify the performance of the software, we tested the sensitivity of the
99　analytical and optimization-based solutions to their input conditions and assessed when each
100　method is most appropriate. To quantify the variability of the fragmentation behavior of an
101　instrument over time, we examined the scrambling behavior of one IRMS over the course of four
102　years of measurements. We derived a simplified equation and used a Monte Carlo simulation
103　approach to quantify the effect of uncertainty in the scrambling coefficients on the final isotope
104　deltas. Finally, we performed an intercalibration using this software across two labs, at Stanford
105　University ('Lab 1') and the University of Basel ('Lab 2'). This paper introduces the theory,
106　practical applications, and testing of pyisotopomer; instructions on how to use pyisotopomer are
107　available in the documentation on the Python Package Index[57].
108
109　**2. Mathematical framework**
110　　　　The molecular ion number ratios 45/44 (^{45}R) and 46/44 (^{46}R) can be written in terms of
111　atomic isotope ratios as[36,53]:

$$^{45}R = {}^{15}R^\alpha + {}^{15}R^\beta + {}^{17}R \tag{3}$$

$$^{46}R = \left({}^{15}R^\alpha + {}^{15}R^\beta\right){}^{17}R + {}^{18}R + {}^{15}R^\alpha {}^{15}R^\beta \tag{4}$$

112　where $^{15}R^\alpha$, $^{15}R^\beta$, ^{17}R and ^{18}R denote the number ratios of $^{14}N^{15}N^{16}O$, $^{15}N^{14}N^{16}O$, $^{14}N_2{}^{17}O$, and
113　$^{14}N_2{}^{18}O$, respectively, to $^{14}N_2{}^{16}O$, assuming a stochastic isotope distribution between mono- and
114　poly-substituted isotopocules.
115　　　　For many N₂O samples, ^{17}R covaries with ^{18}R according to the oxygen isotope ratios of
116　Vienna Standard Mean Ocean Water (VSMOW)[58,59] and a mass-dependent relationship between
117　^{17}R and ^{18}R with coefficient $\beta = 0.516$[60]. Deviations from this relationship are expressed by the
118　oxygen triple isotope excess $\Delta(^{17}O)$[60–62], which provides additional information about the sources
119　and sinks of N₂O[60,63]:

$$^{17}R/^{17}R_{\text{VSMOW}} = \left({}^{18}R/0.0020052\right)^\beta [\Delta(^{17}O) + 1] \tag{5}$$

120        $\Delta(^{17}O)$ is sometimes assumed to be equal to zero but should be measured separately for
121   samples with a significant $\Delta(^{17}O)$ anomaly, such as atmospheric nitrate[60,62,63].
122   The simplest formulation for the NO^+ fragment ion number ratio 31/30 (^{31}R) is given as[36]:

$$^{31}R = {}^{15}R^\alpha + {}^{17}R \tag{6}$$

123   This equation would represent the ^{31}R measured by IRMS if no scrambling occurred.
124   To describe instead the scrambled ^{31}R, Toyoda and Yoshida[36] define the rearrangement
125   factor y (which was later given the symbol γ) as "the fraction of NO^+ bearing the β nitrogen of
126   the initial N_2O to the total NO^+ formed," to yield:

$$^{31}R = (1 - \gamma){}^{15}R^\alpha + \gamma{}^{15}R^\beta + {}^{17}R \tag{7}$$

127   where $^{15}R^\alpha$ and $^{15}R^\beta$ represent atomic isotope ratios of the sample. In other words, γ relates the
128   scrambled NO^+ fragment ratio to the unscrambled $^{15}R^\alpha$ and $^{15}R^\beta$ of the sample.
129   Kaiser et al.[53] introduced a more complete representation of ^{31}R, adding terms for
130   $^{15}N^{15}N^{16}O$, $^{14}N^{15}N^{17}O$, and $^{15}N^{14}N^{17}O$ to m/z 31, and terms for $^{15}N^{14}N^{16}O$ and $^{14}N^{15}N^{16}O$ to m/z
131   30:

$$\begin{aligned}
^{31}R &= (1 - \gamma){}^{15}R^\alpha + \gamma{}^{15}R^\beta + {}^{17}R - \frac{\gamma(1 - \gamma)\left({}^{15}R^\alpha - {}^{15}R^\beta\right)^2}{1 + \gamma{}^{15}R^\alpha + (1 - \gamma){}^{15}R^\beta} \tag{8} \\
&= \frac{(1 - \gamma){}^{15}R^\alpha + \gamma{}^{15}R^\beta + {}^{15}R^\alpha{}^{15}R^\beta + {}^{17}R[1 + \gamma{}^{15}R^\alpha + (1 - \gamma){}^{15}R^\beta]}{1 + \gamma{}^{15}R^\alpha + (1 - \gamma){}^{15}R^\beta}
\end{aligned}$$

132   Note that Kaiser et al.[53] use the symbol "s" for γ, $^{15}R_1$ for $^{15}R^\beta$, and $^{15}R_2$ for $^{15}R^\alpha$.
133   To account for different fragmentation rates of different N_2O isotopocules, Westley et
134   al.[54] replaced the rearrangement factor γ with nine separate coefficients:

$$^{31}R = \frac{a_{31}{}^{15}R^\alpha + b_{31}{}^{15}R^\beta + c_{31}{}^{15}R^\alpha{}^{15}R^\beta + {}^{17}R[d_{31} + e_{31}{}^{15}R^\alpha + f_{31}{}^{15}R^\beta]}{1 + a_{30}{}^{15}R^\alpha + b_{30}{}^{15}R^\beta + c_{30}{}^{15}R^\alpha{}^{15}R^\beta} \tag{9}$$

135   While this approach considers the possibility of different rearrangement factors for every
136   N_2O isotopocule as well as $^{15}N_2^+$ formation, it also requires solving for three to nine coefficients,
137   depending on whether a_{30}, b_{30} and c_{30}, as well as d_{31}, e_{31} and f_{31}, are considered separately from
138   coefficients a_{31}, b_{31} and c_{31}.
139   Frame and Casciotti[50] simplify this equation by reducing the number of rearrangement
140   factors to two coefficients, γ and κ, which represent the yield of $^{14}NO^+$ from $^{14}N^{15}N^{16}O$ and
141   $^{14}N^{15}N^{17}O$, and the yield of $^{15}NO^+$ from $^{15}N^{14}N^{16}O$, respectively. This produces the equation:
142

$$^{31}R = \frac{(1 - \gamma){}^{15}R^\alpha + \kappa{}^{15}R^\beta + {}^{15}R^\alpha{}^{15}R^\beta + {}^{17}R[1 + \gamma{}^{15}R^\alpha + (1 - \kappa){}^{15}R^\beta]}{1 + \gamma{}^{15}R^\alpha + (1 - \kappa){}^{15}R^\beta} \tag{10}$$

143   The important pieces of information contained within the two scrambling factors are the
144   unequal rates of fragmentation for the isotopomers $^{14}N^{15}NO$ and $^{15}N^{14}NO$, which eqns. (7) and
145   (8) assume are equal. Eqn. (10) is formulated by assuming that the ^{17}O-isotopocules have the
146   same scrambling behavior as the ^{16}O-isotopocules, i.e., $e_{31} = 1 - a_{31}$ and $f_{31} = 1 - b_{31}$, in terms of
147   the coefficients in eqn. (9). It is also assumed that $c_{31} = 1$, i.e., the yield of $^{15}N^{16}O^+$ from $^{15}N_2^{16}O$
148   is equal to the yield of $^{14}N^{16}O^+$ from $^{14}N_2^{16}O$. Given that naturally occurring N_2O contains very
149   little $^{15}N_2^{16}O$, a small difference in this yield would not significantly alter ^{31}R[64]. Finally, it is
150   assumed that $d_{31} = 1$, or that the yield of $^{14}N^{17}O^+$ from $^{14}N_2^{17}O$ is equal to the yield of $^{14}N^{16}O^+$
151   from $^{14}N_2^{16}O$; again, an assumption yielding little error in ^{31}R, given the low natural abundance
152   of ^{17}O in N_2O[60].

Eqn. (10) can be rearranged to give an equation for γ as a function of κ (the full derivation is presented in Supplementary text S1):

$$\gamma = \frac{{}^{15}R^\alpha + \kappa\,{}^{15}R^\beta + {}^{15}R^\alpha\,{}^{15}R^\beta - ({}^{31}R - {}^{17}R)\left[1 + (1-\kappa)\,{}^{15}R^\beta\right]}{{}^{15}R^\alpha(1 + {}^{31}R - {}^{17}R)} \tag{11}$$

For two reference materials, we can write two such equations and solve for two unknowns, γ and κ. ${}^{15}R^\alpha$ and ${}^{15}R^\beta$ represent *known* values for each reference material, and ${}^{31}R$ is the observed quantity. Essentially, we are asking what values of γ and κ for a pair of known ${}^{15}R^\alpha$ and ${}^{15}R^\beta$ values gives the observed ${}^{31}R$ for each reference gas. Setting the two solutions for γ equal allows us to determine κ and γ algebraically from the assigned ${}^{15}R$ values of reference materials 1 and 2 (${}^{15}R_1^\alpha$, ${}^{15}R_1^\beta$, ${}^{15}R_2^\alpha$, ${}^{15}R_2^\beta$), their observed ${}^{31}R$ values (${}^{31}R_1$, ${}^{31}R_2$), and the ${}^{17}R$ values (${}^{17}R_1$, ${}^{17}R_2$):

$$\kappa = \frac{\dfrac{\left({}^{15}R_1^\alpha - {}^{31}R_1 + {}^{17}R_1\right)\left(1 + {}^{15}R_1^\beta\right)}{{}^{15}R_1^\alpha(1 + {}^{31}R_1 - {}^{17}R_1)} - \dfrac{\left({}^{15}R_2^\alpha - {}^{31}R_2 + {}^{17}R_2\right)(1 + {}^{15}R_2^\beta)}{{}^{15}R_2^\alpha(1 + {}^{31}R_2 - {}^{17}R_2)}}{\dfrac{{}^{15}R_2^\beta}{{}^{15}R_2^\alpha} - \dfrac{{}^{15}R_1^\beta}{{}^{15}R_1^\alpha}} \tag{12a}$$

$$\gamma = \frac{\dfrac{\left({}^{15}R_1^\alpha - {}^{31}R_1 + {}^{17}R_1\right)\left(1 + {}^{15}R_1^\beta\right)}{{}^{15}R_1^\alpha(1 + {}^{31}R_1 - {}^{17}R_1)}\left(\dfrac{{}^{15}R_2^\beta}{{}^{15}R_2^\alpha}\right) - \dfrac{\left({}^{15}R_2^\alpha - {}^{31}R_2 + {}^{17}R_2\right)\left(1 + {}^{15}R_2^\beta\right)}{{}^{15}R_2^\alpha(1 + {}^{31}R_2 - {}^{17}R_2)}\left(\dfrac{{}^{15}R_1^\beta}{{}^{15}R_1^\alpha}\right)}{\dfrac{{}^{15}R_2^\beta}{{}^{15}R_2^\alpha} - \dfrac{{}^{15}R_1^\beta}{{}^{15}R_1^\alpha}} \tag{12b}$$

After substituting ${}^{45}R - {}^{15}R^\alpha - {}^{15}R^\beta$ for ${}^{17}R$, the equations for γ and κ can also be written as follows:

$$\kappa = \frac{\dfrac{\left({}^{45}R_1 - {}^{31}R_1 - {}^{15}R_1^\beta\right)\left(1 + {}^{15}R_1^\beta\right)}{{}^{15}R_1^\alpha(1 + {}^{15}R_1^\alpha + {}^{15}R_1^\beta + {}^{31}R_1 - {}^{45}R_1)} - \dfrac{\left({}^{45}R_2 - {}^{31}R_2 - {}^{15}R_2^\beta\right)\left(1 + {}^{15}R_2^\beta\right)}{{}^{15}R_2^\alpha(1 + {}^{15}R_2^\alpha + {}^{15}R_2^\beta + {}^{31}R_2 - {}^{45}R_2)}}{\dfrac{{}^{15}R_2^\beta}{{}^{15}R_2^\alpha} - \dfrac{{}^{15}R_1^\beta}{{}^{15}R_1^\alpha}} \tag{13a}$$

$$\gamma = \frac{\dfrac{\left({}^{45}R_1 - {}^{31}R_1 - {}^{15}R_1^\beta\right)\left(1 + {}^{15}R_1^\beta\right)}{{}^{15}R_1^\alpha(1 + {}^{15}R_1^\alpha + R_1^\beta + {}^{31}R_1 - {}^{45}R_1)}\left(\dfrac{{}^{15}R_2^\beta}{{}^{15}R_2^\alpha}\right) - \dfrac{\left({}^{45}R_2 - {}^{31}R_2 - {}^{15}R_2^\beta\right)\left(1 + {}^{15}R_2^\beta\right)}{{}^{15}R_2^\alpha(1 + {}^{15}R_2^\alpha + {}^{15}R_2^\beta + {}^{31}R_2 - {}^{45}R_2)}\left(\dfrac{{}^{15}R_1^\beta}{{}^{15}R_1^\alpha}\right)}{\dfrac{{}^{15}R_2^\beta}{{}^{15}R_2^\alpha} - \dfrac{{}^{15}R_1^\beta}{{}^{15}R_1^\alpha}} \tag{13b}$$

To obtain ${}^{31}R_1$ and ${}^{31}R_2$ in continuous-flow analysis, we measure two reference materials (CA08214 and 53504, Table 1) against a common working reference gas (wr), which is calibrated independently ("Lab 1 pure N_2O direct injection" and "Lab 2 pure N_2O direct injection" in Table 1). The working reference is a third calibrated reference material that normalizes different runs to the same reference frame:

$$^{31}R_1 = \left(1 + {}^{31}\delta_1\right){}^{31}R_{wr} \tag{14}$$

$$^{31}R_2 = \left(1 + {}^{31}\delta_2\right){}^{31}R_{wr} \tag{15}$$

171   where $^{31}R_1$ and $^{31}R_2$ are calculated values that depend on γ and κ, $^{31}\delta$ is the measured ion
172   current ratio difference of sample (1 or 2) to working reference peak, and $^{31}R_{wr}$ is an assumed
173   value calculated with constant γ and κ and assigned $^{15}R^{\alpha}$, $^{15}R^{\beta}$, and ^{17}R. Calculating $^{31}R_{wr}$ with
174   constant γ and κ assumes that the working reference peak experiences a defined scrambling
175   behavior that could differ from that of a sample peak; ultimately, however, $^{31}R_{wr}$ drops out of the
176   final $\delta(^{15}N^{sp})$ calculation, so this assumption has little effect.
177   The "algebraic" solution in pyisotopomer[65] uses $^{31}R_1$ and $^{31}R_2$ in eqns. (11) and (12) to
178   obtain γ and κ. The "least_squares" method in pyisotopomer[65] solves eqns. (14) and (15) for γ
179   and κ iteratively with a least squares optimization routine. We present a full discussion of the
180   appropriate use of the algebraic and least squares methods in section 4.2.
181   Some of the isotopomer literature obtains $^{15}R^{bulk}$ and $^{15}R^{\alpha}$ by regression between true and
182   measured values of reference materials, inferring $^{15}R^{\beta}$ indirectly[20]. In this case, a linear
183   calibration curve replaces the scrambling correction. However, a linear calibration curve just
184   based on "known" $\delta(^{15}N^{\alpha})$ values will fail unless the "known" $\delta(^{15}N^{sp})$ values are constant — in
185   other words, a linear calibration curve is only acceptable if the unknowns are close in their
186    $\delta(^{15}N^{sp})$ to those of the reference material. It is not accurate if unknowns diverge in their $\delta(^{15}N^{sp})$
187   from that of the reference material(s). This is because the measured $^{31}\delta$ value depends on both
188    $^{15}R^{\alpha}$ and $^{15}R^{\beta}$ (Supplementary text S2).
189   To obtain $^{15}R^{\alpha}$, $^{15}R^{\beta}$, and ^{18}R of unknowns, pyisotopomer solves for these values from
190   eqns. (3), (4), (5), and (10), using ^{31}R, ^{45}R, ^{46}R, γ, and κ as input terms[50]. The delta values $\delta(^{15}N^{\alpha})$,
191    $\delta(^{15}N^{\beta})$, $\delta(^{15}N^{sp})$, $\delta(^{15}N^{bulk})$, and $\delta(^{18}O)$ are calculated from $^{15}R^{\alpha}$, $^{15}R^{\beta}$, and ^{18}R relative to primary
192   reference scales (^{15}R from atmospheric N_2, ^{17}R and ^{18}R from VSMOW; if desired, the values of
193   primary reference scale ratios may be adjusted with keyword arguments, as described in the
194   pyisotopomer Documentation[65]). Additionally, if $\Delta^{17}O$ has been measured separately[60,62,63],
195   pyisotopomer can take this value into account in the calculation of $\delta(^{15}N^{\alpha})$, $\delta(^{15}N^{\beta})$, $\delta(^{15}N^{sp})$,
196    $\delta(^{15}N^{bulk})$, and $\delta(^{18}O)$.
197
198   **3. Experimental methods**
199   **3.1 Preparation and analysis of dissolved N_2O reference materials**
200   A series of dissolved N_2O reference materials (Table 1) were prepared and analyzed in
201   both Lab 1 and Lab 2. Reference materials were prepared by filling 160-mL glass serum bottles
202   (Wheaton) with de-ionized water and removing a 4-mL headspace (Lab 1) or 10 to 20-mL
203   headspace (Lab 2), then capped with a gray butyl rubber septum (National Scientific) and sealed
204   with an aluminum crimp seal. These bottles were purged with helium for 90 minutes at yields a
205   minimum flow rate of 100 mL/min to remove all background N_2O. The purged bottles were then
206   injected with 2 to 43 nmol N_2O to give N_2O concentrations of 13 to 275 nM (Lab 1) or 1 to 60
207   nmol N_2O to give N_2O concentrations of 6 to 427 nM (Lab 2) in a matrix of He or synthetic air
208   (Table 1) using a gas-tight syringe. Reference materials prepared in Lab 1 were preserved with
209   100 µL saturated mercuric chloride ($HgCl_2$) solution; those prepared in Lab 2 contained no
210   added preservative. For Lab 1, atmosphere-equilibrated seawater was prepared by filtering
211   surface seawater (collected in Half Moon Bay, CA) through a 0.22 mm Sterivex filter, allowing
212   it to undergo static equilibration with outdoor air for three days, then re-filtering into 160-mL
213   serum bottles, removing a 1-mL headspace, and preserving with 100 µL saturated mercuric

chloride solution. For Lab 2, atmosphere-equilibrated reference materials were prepared by purging either de-ionized water or a sodium chloride solution with helium, allowing it to undergo static equilibration with outdoor air for three days, filling into 160-mL serum bottles, and removing a 10-mL headspace. While we were able to correct for these differences in reference material preparation, future intercalibration efforts should aim to prepare reference materials the same way in participating laboratories. In addition, the linearity relationships should be determined from analyzing different amounts of gaseous reference materials, to separate any artifacts due to preparation and extraction of dissolved N_2O reference materials from the abundance linearity of the isotope ratio mass spectrometer itself.

Reference materials were run in the same format as samples to account for any potential fractionation associated with the purge-and-trap system. The magnitude of such fractionation was quantified for Lab 1 by running aliquots of the pure N_2O reference tank in sample format; this test yielded offsets of (0.22 ± 0.52) ‰ for $\delta(^{15}N^{bulk})$ and (0.16 ± 0.62) ‰ for $\delta(^{18}O)$ vs. the reference tank injection (see Supplementary text S3 for a full discussion of potential fractionation effects in the purge-and-trap system).

The reference gases were calibrated independently by J. Mohn (EMPA; mini-QCLAS aerodyne) or S. Toyoda (Tokyo Tech; IRMS), except for one internal standard used by Lab 1 (B6; Table 1). The $\delta(^{17}O)$ values for each gas were calculated assuming a mass-dependent relationship between ^{17}R and ^{18}R (eqn. 5).

Reference gases and samples were measured on Thermo Finnigan DELTA V Plus isotope ratio mass spectrometers (IRMS; Thermo Fisher Scientific, Waltham, MA) in Labs 1 and 2. Each IRMS had Faraday cups configured to simultaneously measure m/z 30, 31, 44, 45, and 46. The measurements from the Lab 1 DELTA V Plus were made under normal operating conditions, using an ionization energy of 124 eV, accelerating voltage of 3 kV, emission current of 1.50 mA, and box and trap currents of 0.68 and 0.82 mA, respectively. The measurements from the Lab 2 DELTA V Plus were made under normal operating conditions, using an ionization energy of 110 eV, accelerating voltage of 3 kV, emission current of 1.00 mA, and box and trap currents of 0.45 and 0.55 mA, respectively. Reference materials and samples were analyzed on custom purge-and-trap systems coupled to each IRMS, which was run in continuous flow mode[66] (Table 1). The two systems had slight differences in the purge-and-trap method: in Lab 1, liquid from each sample bottle was transferred under helium pressure to a sparging column to extract the dissolved gases[67]; in Lab 2, each sample was extracted by purging directly from the bottle. The effects of these differences are discussed further in Results and Discussion.

3.2 Data corrections
3.2.1 Linearity relation

The measured ion current ratios 31/30, 45/44, and 46/44 of each sample peak were divided by those of the working reference peak. This produced three molecular isotope delta values $^{31}\delta+1$, $^{45}\delta+1$, and $^{46}\delta+1$, where $\delta = R_s/R_{wr} - 1$, with the subscripts "s" and "wr" denoting sample and working reference, respectively (Figure 1, Step 5).

The δ values were corrected for the effect of peak size[33]. For Lab 1, this was accomplished by running six reference materials (reference gases S2, B6, A01, CA06261, 90454, and 94321; Table 1) in size series ranging from 2-43 nmol N_2O. For Lab 2, three reference materials (CA06261, 53504, and CA08214) were run in size series ranging from 1-60 nmol N_2O (Figure 1, Step 6).

259   To obtain a single size correction slope from multiple size series, we used the dummy-
260 variable method of combining regressions[68]. The dummy variable method is an improvement
261 over simply averaging each individually calculated slope because it implicitly weighs each size
262 series by its informativeness, producing a slope that is more likely to reflect the overall linearity
263 behavior of the instrument[68]. For a given material, each measured $\delta+1$ is a linear function of its
264 peak area (A) plus an intercept ($\gamma_1 + \gamma_2 D_2 + \gamma_3 D_3$):

$$\delta + 1 = \hat{\beta}A + \gamma_1 + \gamma_2 D_2 + \gamma_3 D_3 \tag{16}$$

265 where $\hat{\beta}$ represents the regression coefficient for a particular peak area (for m/z 31,45, or 46),
266 obtained by multiple linear regression. The intercept for reference material 1 is γ_1. D_2 and D_3 are
267 'dummy variables' to adjust γ_1 by an appropriate intercept for reference material 2 ($\gamma_1 + \gamma_2$) and
268 reference material 3 ($\gamma_1 + \gamma_3$). Thus, for reference material 1, $D_2 = D_3 = 0$; for reference material
269 2, $D_2 = 1$ and $D_3 = 0$; for reference material 3, $D_2 = 0$ and $D_3 = 1$. These dummy variables allow
270 us to obtain one slope for each isotope delta from multiple datasets accounting for differences in
271 intercept, with each reference material weighted by its spread in the x-axis range. Thus, slopes
272 $\hat{\beta}_{31}$, $\hat{\beta}_{45}$, and $\hat{\beta}_{46}$ were calculated for $^{31}\delta+1$, $^{45}\delta+1$, and $^{46}\delta+1$, respectively, each using eqn. (16).
273   To normalize measured values of $\delta+1$ to a common peak area, we first calculated the
274 $(\delta+1)_0$ that would be measured at m/z 44 peak area A_0:

$$(\delta + 1)_0 = \hat{\beta}(A_0) + \gamma_1 + \gamma_2 D_2 + \gamma_3 D_3 \tag{17}$$

275 Note that $(\delta+1)_0$ is still a function of $\hat{\beta}$, the intercepts γ_1, γ_2, γ_3, and the dummy variables D_2 and
276 D_3. To obtain the difference $\delta_0 - \delta$ from the measured m/z 44 peak area A, we subtract eqn. (17)
277 from eqn. (16), to obtain:

$$(\delta + 1)_0 - (\delta + 1) = \hat{\beta}(A_0 - A)$$

278 In this case, the size-corrected molecular isotope ratio, δ_0, for each sample with measured δ and
279 peak area A is given by:

$$(\delta + 1)_0 = \hat{\beta}(A_0 - A) + (\delta + 1) \tag{18}$$

280 Eqn. (18) is simply a function of the slope $\hat{\beta}$, the measured (A) and target (A_0) m/z 44 peak areas,
281 and the measured δ. Thus, eqn. (18) can be applied across a range of peak areas and δ values to
282 normalize these δ values to a common peak area. Using this method, we normalized the
283 measured $^{31}\delta+1$, $^{45}\delta+1$, and $^{46}\delta+1$ of each sample to a peak area (A_0) of 20 Vs (volt seconds),
284 equivalent to 10 nmol N_2O on the Lab 1 IRMS (Figure 1, Step 7). We note that the linearity
285 correction estimated here implicitly assumes that samples and reference materials are affected by
286 the same relative blank size.
287
288 **3.2.2 Scale normalization and calculation of ^{17}R**
289   After applying the linearity correction, a scale normalization was applied to $^{45}\delta$ and $^{46}\delta$
290 (Figure 1, Step 8). The scale normalization for $^{45}\delta$ and $^{46}\delta$ needs to be carried out before the
291 scrambling correction (which is essentially a scale normalization of $^{31}\delta$); otherwise, the wrong
292 bulk $^{15}N/^{14}N$ and $^{18}O/^{16}O$ ratios are implied. Furthermore, while the γ and κ calculations
293 constrain the differences between $\delta(^{15}N^{\alpha})$ and $\delta(^{15}N^{\beta})$, their absolute values are governed by
294 $\delta(^{15}N^{bulk})$, necessitating that the "correct", normalized value of $^{45}\delta$ be input to the scrambling
295 equations. This scale normalization is a replacement for any scale normalization or offset
296 correction to the final output δ values, such as the one-point and two-point offset corrections
297 calculated and applied in Mohn et al. (2014).
298   A scale normalization was calculated for each run included in the intercalibration
299 exercise. Since assigned values of ^{45}R and ^{46}R for each reference gas were unavailable, assigned

300   ^{45}R and ^{46}R were calculated from assigned $^{15}R^{\alpha}$, $^{15}R^{\beta}$, and ^{18}R and eqns. (3), (4), and (5) (Table
301   1), assuming $^{17}R_{VSMOW} = 0.00037996^{[69]}$ and $^{18}R_{VSMOW} = 0.0020052^{[58]}$. Next, the assigned ^{45}R and
302   ^{46}R for each reference gas were divided by the known ^{45}R and ^{46}R of the direct N_2O reference
303   injection to obtain assigned $^{45}\delta$ and $^{46}\delta$ for each reference material. Then, these assigned $^{45}\delta$ and
304    $^{46}\delta$ values were compared to measured $^{45}\delta$ and $^{46}\delta$ values, and scale normalization coefficients
305   were calculated following the logarithmic scale normalization outlined in Kaiser et al. (2007):

306
$$\ln(1 + {}^{45}\delta^n) = m\ln(1 + {}^{45}\delta) + b$$

307   where $^{45}\delta^n$ is the normalized $^{45}\delta$, "m" is the slope of the regression of $\ln(1+{}^{45}\delta^n)$ vs.
308    $\ln(1+{}^{45}\delta)$, and "b" is the intercept (and likewise for $^{46}\delta$). From this regression, the normalized δ
309   values can be obtained:

$$1 + {}^{45}\delta^n = e^b(1 + {}^{45}\delta)^m \tag{19}$$

310   For the working reference, the values of $^{45}\delta$ and $^{45}\delta^n$ are equal to zero, so the intercept b
311   should be equal to or very close to zero. The benefit of the logarithmic normalization is that,
312   unlike a linear scale normalization, it is scale-invariant[62]: essentially, the logarithmic scale
313   normalization does not skew the data towards extremely high or low values, and instead equally
314   weights all data points[62].
315   Next, a measured ^{18}R was derived from the scale-normalized ^{45}R and ^{46}R for each sample
316   and reference material (Figure 1, Step 8). The size correction and scale normalization were
317   carried out in the pyisotopomer spreadsheet template; the ^{18}R derivation from the scale-
318   normalized ^{45}R and ^{46}R was the first step accomplished by the pyisotopomer code[65]. Deriving ^{18}R
319   was accomplished by assuming a mass-dependent relationship between ^{17}R and ^{18}R (eqn. 5) and
320    $^{15}R^{\alpha} = {}^{15}R^{\beta} = {}^{15}R^{bulk}$. These terms are then substituted into eqns. (3) and (4) to yield:

$$^{45}R = 2\,{}^{15}R^{bulk} + {}^{17}R_{VSMOW}\left(\frac{{}^{18}R}{{}^{18}R_{VSMOW}}\right)^{\beta}(\Delta^{17}O + 1) \tag{20}$$

$$^{46}R = {}^{18}R + 2\,{}^{15}R^{bulk}\left[{}^{17}R_{VSMOW}\left(\frac{{}^{18}R}{{}^{18}R_{VSMOW}}\right)^{\beta}(\Delta^{17}O + 1)\right] + \left({}^{15}R^{bulk}\right)^2 \tag{21}$$

321   Note that the slope β of the mass-dependent relationship between ^{17}R and ^{18}R is an
322   adjustable parameter in the code (default: 0.516), and $\Delta^{17}O$ for each reference material may be
323   entered in the data correction template and subsequently accounted for in this correction (default:
324   0 ‰). Eqns. (20) and (21) were then solved for ^{18}R and $^{15}R^{bulk}$ to obtain an estimated ^{18}R and
325    $^{15}R^{bulk}$ for each sample and reference material, and ^{17}R was calculated from ^{18}R according to eqn.
326   (5). The resulting ^{18}R, ^{17}R, and $^{15}R^{bulk}$ were used in the scrambling calculation. They contain an
327   error due to the assumption that $^{15}R^{\alpha} = {}^{15}R^{\beta} = {}^{15}R^{bulk}$, although the magnitude of this error should
328   be small[62]. Later, the isotopomer calculation solves for $^{15}R^{\alpha}$ and $^{15}R^{\beta}$ separately and thus corrects
329   this error.
330   In the intercalibration exercise, values of m and b were calculated from the slopes of
331   assigned $^{45}\delta^a$ vs. measured $^{45}\delta$ and assigned $^{46}\delta^a$ vs. measured $^{46}\delta$ from the reference materials in
332   each run. These runs took place in February 2021 for Lab 1 and August 2020 and November
333   2020 for Lab 2. Combined, the scale normalization and size correction should account for any
334   size- or isotope-ratio dependent effects, including those of a blank, linearity, or fractionation in
335   the GasBench.
336
337   **3.2.3 Calculating $^{31}R_m$ of the direct N_2O reference injection**

338 We used the same scrambling coefficients for the working reference gas as for the
339 samples. We recommend that the user calculates the ^{31}R of the direct reference injection ($^{31}R_{wr}$ in
340 eqns. 14 and 15) with the following sequence of steps: 1) calculate $^{31}R_{wr}$ from eqn. (10) with
341 either $\gamma = \kappa = 0.1$, which reflects commonly reported values[36,50,54], or an *a priori* estimate, if
342 available (Figure 1, Step 9); 2) use that $^{31}R_{wr}$ to correct data from two reference materials and
343 from those reference materials, obtain γ and κ from eqns. (11) and (12) (Figure 1, Step 10); 3)
344 use these updated γ and κ to re-calculate $^{31}R_{wr}$ from eqn. (10) (Figure 1, Step 11). The input γ and
345 κ (used to calculate $^{31}R_{wr}$) and output γ and κ (calculated from paired reference materials) should
346 converge quickly, so one iteration of this process should be sufficient. This value of $^{31}R_{wr}$ can
347 then be used to convert $^{31}\delta$ to $^{31}R_s$. The user should also note that there are likely to be multiple
348 pairings of input and output γ and κ that will consistently yield indistinguishable delta values**.**
349
350 ### 3.2.4 IRMS scrambling calibration and isotopomer calculation
351 The "Scrambling" function of pyisotopomer was used to calculate γ and κ algebraically
352 from all possible pairings of reference materials CA08214 and 53504 measured on a given IRMS
353 (Lab 1 or Lab 2; Figure 1, Step 13). The reference materials CA08214 and 53504 were chosen
354 because of their 113 ‰ $\delta(^{15}N^{sp})$ difference (see Results and Discussion for a description of how
355 to choose reference material pairings), as well as the range of $\delta(^{15}N^{\alpha})$, $\delta(^{15}N^{\beta})$, $\delta(^{15}N^{bulk})$, and
356 $\delta(^{18}O)$ spanned by the two reference materials, which represent values found typically in
357 culture[52,70] and nature[26,31]. One-week running averages of γ and κ were calculated to smooth their
358 variation and used to obtain position-dependent δ values for unknowns and reference materials
359 run as unknowns for quality control (CA06261, S2, B6, and atmosphere-equilibrated seawater),
360 using the "Isotopomers" function of pyisotopomer (Figure 1, Step 14).
361 For comparison, this exercise was repeated, calculating γ and κ iteratively with the least
362 squares optimization (Figure 1, Step 12). The mean algebraic γ and κ from the paired reference
363 materials CA08214 and 53504 was used as the initial guess for the least squares solver. In this
364 case, reference materials CA08214 and CA06261 were used to calculate the least squares γ and
365 κ, because these reference materials are close in their calibrated isotopomer values to natural
366 abundance unknowns. As above, γ and κ were combined into a one-week running average; these
367 running averages of γ and κ for each system were used to obtain position-dependent δ values for
368 reference materials and unknowns in the intercalibration exercise (Figure 1, Step 14). The
369 analytical precisions of $\delta(^{15}N^{\alpha})$, $\delta(^{15}N^{\beta})$, $\delta(^{15}N^{sp})$, $\delta(^{15}N^{bulk})$, and $\delta(^{18}O)$ produced by each method
370 are presented in the Results and Discussion.
371 N_2O amounts were obtained from the m/z 44 peak area and instrument N_2O sensitivity[67].
372 To obtain the conversion factor between peak area and amount of N_2O, the peak areas for
373 reference material amounts from 1 to 40 nmol N_2O were recorded. Standard deviations for
374 inferred N_2O amounts of replicate unknown samples were 0.07 nmol for Lab 1, and 0.19 nmol
375 for Lab 2. All data corrections are described in the README documents associated with
376 pyisotopomer on the Python Package Index[65].
377
378 ### 3.3 Lake water unknowns
379 To validate the scrambling calibration, samples of unknown isotopic composition were
380 collected from Lake Lugano, Switzerland in July 2020 and analyzed separately by both Lab 1
381 and Lab 2. The samples were collected at depths of 10 and 90 meters, including six replicate
382 bottles at each depth. Samples were collected into 160-mL glass serum bottles (Wheaton),
383 overflowing each bottle twice, closing bubble-free, and removing liquid to form a 10-mL

384 headspace comprised of air. Based on the northern hemisphere monthly mean tropospheric N_2O
385 mole fraction when the samples were collected in July, 2020[71], an atmospheric headspace of this
386 volume would have contained 0.13 nmol N_2O. For Lab 2, where the full amount of N_2O in the
387 sample is measured, incorporation of the headspace into the measurement results in a 0.13 nmol
388 overestimation of the amount of N_2O in the sample[71]. For Lab 1, where 2 mL sample liquid is
389 left behind post-analysis, equilibration the 10-mL headspace during sample storage results in
390 either an underestimate (0.12 nmol) or overestimate (0.10 nmol) of N_2O in the sample,
391 depending on its concentration. In both cases, these errors are similar to the analytical precision
392 of the N_2O amount measurement. Each sample was capped with a gray butyl septum (National
393 Scientific) and sealed with an aluminum crimp seal. Samples were promptly preserved with 100
394 µL saturated mercuric chloride solution and stored at lab temperature (20-22°C). The isotope
395 fractionation associated with N_2O partitioning, defined as the isotope ratio of the gas phase
396 divided by the isotope ratio of the liquid phase, ($^{15}\varepsilon = -0.7$ ‰, $^{18}\varepsilon = -1.1$ ‰, 298.2 K) falls
397 within the analytical uncertainty[72]. The six replicate bottles at each depth were split into two
398 groups of three replicate bottles to be measured by Lab 1 and Lab 2, respectively.
399
400 **4. Results and Discussion**
401
402 **4.1 Linearity relation**
403   Linearity relations were calculated using the dummy variable method described in
404 Section 3.2.1 and applied to the intercalibration data as follows. A linearity relation was
405 determined for Lab 1 in February 2021 (Figure 2a-c) and applied to lake water samples run in
406 Lab 1 and reference materials prepared and run in Lab 1. Reference materials prepared in Lab 2
407 but run in Lab 1 exhibited statistically distinct linearity slopes from those both prepared and run
408 in Lab 1; thus, a separate linearity relation was applied to these reference materials (but not to the
409 lake water samples) (Figure 2d-f). A linearity relation was determined for Lab 2 in May 2020
410 (Figure 2g-i) and applied to lake water samples and reference materials run in Lab 2. As
411 previously observed[73], for each linearity relation, the slopes of the fits for individual reference
412 materials were identical within error. The linearity correction reduced the spread of measured
413 molecular isotope ratios across size series of each given reference material (Figure S2).
414
415 **4.2 IRMS scrambling calibration**
416   For both labs, the "algebraic" solution produced reasonable values of γ and κ (i.e.,
417 between 0 and 1) for reference material pairings involving the reference material 53504 ($\delta(^{15}N^{sp})$
418 $= -93$ ‰). The mean γ and κ calculated for Lab 1 from reference materials 53504 and CA08214
419 were 0.174±0.022 and 0.083±0.022, respectively (Table S2). In August 2020, the mean γ and κ
420 calculated for Lab 2 from the same two reference materials were 0.095±0.011 and 0.091±0.010,
421 respectively (Table S2). In November 2020, γ and κ for Lab 2 were slightly different but within
422 1σ of the values measured in August 2020 (0.091±0.013 and 0.086±0.013, respectively; Table
423 S2). Other reference materials paired with 53504 produced similar values of γ and κ. The
424 difference $\gamma - \kappa$ was also consistent for reference material pairings with 53504: for Lab 1, $\gamma - \kappa$
425 was 0.090-0.091, and for Lab 2, it was 0.003-0.005 (Table S2).
426   For pairings with 53504, the $\delta(^{15}N^{sp})$ difference between both reference materials was
427 greater than 100 ‰. Pairs of reference materials with smaller $\delta(^{15}N^{sp})$ differences produced more
428 variable γ and κ values with the algebraic solution, which sometimes fell outside the physically
429 plausible range between 0 and 1. For example, in Lab 1, the pairing of CA06261 and CA08214

pyisotopomer   11

produced γ and κ values of 0.01 ± 0.23 and -0.08 ± 0.23, respectively. In this case, the
measurement uncertainty was too large — and the $\delta(^{15}N^{sp})$ values too close — for the scrambling
coefficients to be adequately determined. What matters, however, is that the difference between γ
and κ is accurate; as the results show, the absolute values are less important (and can even be
negative, greater than 1, or otherwise "unphysical").

To understand the uncertainty in γ and κ calculated from equations 11 and 12, we define a
variable d, which allows us to express the analytical solution for γ and κ (eqns. 13a and 13b) in
terms of $\delta(^{15}N^{sp})$, $\delta(^{15}N^{sp})$, and $\delta(^{15}N^{sp})$:

$$d = \frac{\left(^{15}R^{\beta} + {}^{31}R - {}^{45}R\right)\left(1 + {}^{15}R^{\beta}\right)}{{}^{15}R_{\text{atm}}\left(1 + {}^{15}R^{\alpha} + {}^{15}R^{\beta} + {}^{31}R - {}^{45}R\right)} \tag{22}$$

The value of d is similar for all samples and reference gases run on a given IRMS and
depends primarily on the difference ${}^{31}R - {}^{45}R$. Using δ notation, i.e., $\delta(^{15}N) = {}^{15}R/^{15}R_{\text{atm}} - 1$, and
dropping the label "${}^{15}N$" for brevity, eqns. (13a) and (13b) can be written as follows:

$$\kappa = \frac{\dfrac{d_2}{1 + \delta_2^{\alpha}} - \dfrac{d_1}{1 + \delta_1^{\alpha}}}{\dfrac{1 + \delta_2^{\beta}}{1 + \delta_2^{\alpha}} - \dfrac{1 + \delta_1^{\beta}}{1 + \delta_1^{\alpha}}} = \frac{\dfrac{d_2}{1 + \delta_2^{\alpha}} - \dfrac{d_1}{1 + \delta_1^{\alpha}}}{\dfrac{\delta_1^{sp}}{1 + \delta_1^{\alpha}} - \dfrac{\delta_2^{sp}}{1 + \delta_2^{\alpha}}} \tag{23a}$$

$$\gamma = \frac{\dfrac{d_2}{1 + \delta_2^{\alpha}}\left(\dfrac{1 + \delta_1^{\beta}}{1 + \delta_1^{\alpha}}\right) - \dfrac{d_1}{1 + \delta_1^{\alpha}}\left(\dfrac{1 + \delta_2^{\beta}}{1 + \delta_2^{\alpha}}\right)}{\dfrac{1 + \delta_2^{\beta}}{1 + \delta_2^{\alpha}} - \dfrac{1 + \delta_1^{\beta}}{1 + \delta_1^{\alpha}}}$$

$$= \frac{\dfrac{d_2}{1 + \delta_2^{\alpha}}\left(\dfrac{1 + \delta_1^{\beta}}{1 + \delta_1^{\alpha}}\right) - \dfrac{d_1}{1 + \delta_1^{\alpha}}\left(\dfrac{1 + \delta_2^{\beta}}{1 + \delta_2^{\alpha}}\right)}{\dfrac{\delta_1^{sp}}{1 + \delta_1^{\alpha}} - \dfrac{\delta_2^{sp}}{1 + \delta_2^{\alpha}}} \tag{23b}$$

The denominators of these expressions can be approximated by the difference $\delta_1^{sp} - \delta_2^{sp}$.
Thus, if the site preferences of the reference gases are similar, the value of the denominator
approaches zero and the solutions will become uncertain due to the finite measurement error.
Then, the question arises, how far apart must the site preferences of the reference materials be to
obtain robust solutions?

The general form of uncertainty propagation in a variable a with respect to the
observations (y_i) is given by the following equation[74]:

$$\sigma_a^2 = \sum_i \sigma_i^2 \left(\frac{\partial a}{\partial y_i}\right)^2$$

where σ_a is the uncertainty in a, y_i is an individual observation, and σ_i is the uncertainty in the
observation y_i. Ignoring the uncertainties in ${}^{45}R$ and the assigned position-dependent ${}^{15}R$ values,
the uncertainty in κ can be calculated as:

$$\sigma_\kappa^2 = \sigma_{{}^{31}R_1}^2 \left(\frac{\partial \kappa}{\partial {}^{31}R_1}\right)^2 + \sigma_{{}^{31}R_2}^2 \left(\frac{\partial \kappa}{\partial {}^{31}R_2}\right)^2$$

454

$$\frac{\partial \kappa}{\partial^{31}R_1} = \frac{\dfrac{-(1 + {}^{15}R_1^\alpha)(1 + {}^{15}R_1^\beta)}{{}^{15}R_1^\alpha(1 + {}^{15}R_1^\alpha + R_1^\beta + {}^{31}R_1 - {}^{45}R_1)^2}}{\dfrac{\delta_1^{sp}}{1 + \delta_1^\alpha} - \dfrac{\delta_2^{sp}}{1 + \delta_2^\alpha}} \approx \frac{-1}{{}^{15}R_1^\alpha(\delta_1^{sp} - \delta_2^{sp})}$$

455

$$\frac{\partial \kappa}{\partial^{31}R_2} = \frac{\dfrac{-(1 + {}^{15}R_2^\alpha)(1 + {}^{15}R_2^\beta)}{{}^{15}R_2^\alpha(1 + {}^{15}R_2^\alpha + R_2^\beta + {}^{31}R_2 - {}^{45}R_2)^2}}{\dfrac{\delta_1^{sp}}{1 + \delta_1^\alpha} - \dfrac{\delta_2^{sp}}{1 + \delta_2^\alpha}} \approx \frac{-1}{{}^{15}R_2^\alpha(\delta_1^{sp} - \delta_2^{sp})}$$

456

457

458 Assuming $\sigma_{{}^{31}R}/{}^{15}R^\alpha = \sigma_{{}^{31}R_1}/{}^{15}R_1^\alpha = \sigma_{{}^{31}R_2}/{}^{15}R_2^\alpha$, then

459
$$\sigma_\kappa^2 \approx 2\left(\frac{\sigma_{{}^{31}R}}{{}^{15}R^\alpha}\right)^2\left(\frac{1}{\delta_1^{sp} - \delta_2^{sp}}\right)^2$$

460 or

$$\sigma_\kappa \approx \sqrt{2}\frac{\sigma({}^{31}R)}{{}^{15}R^\alpha}\frac{1}{\left|\delta_1^{sp} - \delta_2^{sp}\right|} \tag{24a}$$

461 Similarly, for γ:

$$\sigma_\gamma \approx \sqrt{2}\frac{\sigma({}^{31}R)}{{}^{15}R^\beta}\frac{1}{\left|\delta_1^{sp} - \delta_2^{sp}\right|} \tag{24b}$$

462   where $\sigma({}^{31}R)/{}^{15}R$ can be approximated by the measurement uncertainty in ${}^{31}\delta$ and
463 $\left|\delta_1^{sp} - \delta_2^{sp}\right|$ is the absolute value of the difference in assigned site preferences between the two
464 reference materials. This means that for a measurement uncertainty in ${}^{31}\delta$ of 1 ‰ and a $\delta({}^{15}N^{sp})$
465 difference of 10 ‰ between the two reference materials, γ and κ would have absolute
466 uncertainties of 0.14. This uncertainty translates into a relative uncertainty of about 30 % for the
467 $\delta({}^{15}N^{sp})$ value of an unknown sample – far too high for practical applications (Supplementary
468 text S4). A $\delta({}^{15}N^{sp})$ difference of 100 ‰ would give a more useful absolute uncertainty of 0.014
469 for γ and κ.
470   These theoretical uncertainties are reflected in the experimental data. For Lab 1, the
471 reference materials 53504 ($\delta({}^{15}N^{sp})$ = –92.73 ‰) and CA08214 ($\delta({}^{15}N^{sp})$ = 20.54 ‰) yielded γ =
472 0.174±0.022 and κ = 0.083±0.022. The standard deviation of ${}^{31}\delta$ was 1.89 ‰ (n = 12). This
473 produces an estimated uncertainty in γ and κ of $\sqrt{2}$(1.89 ‰)/(113.27 ‰) = 0.024, which agrees
474 well with the experimental data. Similarly, reference materials 53504 and CA06261 ($\delta({}^{15}N^{sp})$ =
475 27.07 ‰) yielded γ = 0.163±0.018 and κ = 0.073±0.018. The standard deviation of ${}^{31}\delta$ was 1.58
476 ‰ (n = 10), and the $\delta({}^{15}N^{sp})$ difference was 119.80 ‰. This produced an estimated uncertainty in
477 γ and κ of $\sqrt{2}$(1.58 ‰)/(119.80 ‰) = 0.019, also in line with the uncertainties in γ and κ.
478   Rearranging eqns. (24a) and (24b), we obtain expressions for the required $\left|\delta_1^{sp} - \delta_2^{sp}\right|$ to
479 obtain a target level of uncertainty (σ) in γ and κ, given the measurement uncertainty in ${}^{31}R$:

$$\left|\delta_1^{\mathrm{sp}} - \delta_2^{\mathrm{sp}}\right| = \sqrt{2}\,\frac{\sigma(^{31}R)}{^{15}R^\alpha}\frac{1}{\sigma_\kappa} \tag{25a}$$

480

$$\left|\delta_1^{\mathrm{sp}} - \delta_2^{\mathrm{sp}}\right| = \sqrt{2}\,\frac{\sigma(^{31}R)}{^{15}R^\beta}\frac{1}{\sigma_\gamma} \tag{25b}$$

481   Assuming $\sigma(^{31}R)/^{15}R^\alpha \approx \sigma(^{31}R)/^{15}R^\beta \approx \sigma(^{31}\delta)$, we obtain:

$$\left|\delta_1^{\mathrm{sp}} - \delta_2^{\mathrm{sp}}\right| = \sqrt{2}\,\sigma(^{31}\delta)\frac{1}{\sigma_{\gamma\kappa}} \tag{26}$$

482

483   where $\sigma(^{31}\delta)$ is the $^{31}\delta$ measurement uncertainty in per mil, and $\sigma_{\gamma\kappa}$ is the target absolute
484   uncertainty in γ and κ. For example, with a measurement uncertainty of 1 ‰ in $^{31}\delta$, the $\delta(^{15}\mathrm{N}^{\mathrm{sp}})$
485   values of the two reference materials must differ by at least 141 ‰ to achieve an absolute
486   uncertainty in γ and κ of 0.01. Based on these results, we recommend calculating γ and κ from
487   reference materials with a large $\delta(^{15}\mathrm{N}^{\mathrm{sp}})$ difference, as estimated from eqn. (26).
488   As an alternative to the algebraic solution, a least squares optimization can be used to
489   find a solution for γ and , although that solution may find a local optimum rather than a global
490   optimum. The user can select a least squares optimization instead of the algebraic solution with
491   the "method" keyword argument to pyisotopomer's Scrambling function. The least squares
492   optimization smooths measurement uncertainty, making it useful for for fitting repeat
493   measurements of reference materials to a single pair of "best" values for γ and κ. Its disadvantage
494   is that, unlike the algebraic solution, the least squares optimization depends on the initial guess
495   for γ and κ. Using data from reference materials CA06261 and CA08214, a range of initial
496   guesses from $\gamma = \kappa = 0.000$ to $\gamma = \kappa = 0.200$ produced a range of least squares solutions, from $\gamma =$
497   0.090 and $\kappa = 0.000$ to $\gamma = 0.269$ and $\kappa = 0.183$ (Figure S3). Despite this range of γ and κ,
498   however, the least squares optimization produced a consistent $\gamma - \kappa$ of 0.09. As shown in Section
499   4.4, $\gamma - \kappa$ governs the accuracy of $\delta(^{15}\mathrm{N}^{\mathrm{sp}})$ far more than the individual values of γ and κ.
500   Given an accurate initial guess, the least squares optimization will find a minimum at or
501   close to this initial guess, even for reference material pairings close in their $\delta(^{15}\mathrm{N}^{\mathrm{sp}})$. For
502   example, when we used the algebraic γ and κ from reference materials CA08214 and 53504 as an
503   initial guess, the least squares optimization produced similar γ and κ for a variety of reference
504   material pairings (Table S2). Furthermore, for the same initial guess, the least squares
505   optimization finds different solutions for the Lab 1 and Lab 2 instruments, even for reference
506   material pairings close in their $\delta(^{15}\mathrm{N}^{\mathrm{sp}})$ (Table S3). This demonstrates that, depending on the
507   measurement precision at the time, the least squares optimization searches an appropriately wide
508   solution space to resolve large differences in instrument behavior.
509   If the first-time user wishes to obtain accurate individual values of γ and κ, we
510   recommend obtaining reference materials different enough in their $\delta(^{15}\mathrm{N}^{\mathrm{sp}})$ to calculate γ and κ
511   with the algebraic solution. If the user wishes to take advantage of the smoothing of the least
512   squares optimization, this algebraic γ and κ can then be used as the initial guess for the least
513   squares solver.
514   We also recommend that the user test the accuracy of the least squares γ and κ by
515   plugging γ and κ back into eqn. (10) and comparing the result to the measured ^{31}R for each
516   reference material. The two ^{31}R values should match. pyisotopomer[65] performs this calculation
517   automatically and outputs the difference as a δ value:

$$^{31}\delta^{\text{error}} = \frac{^{31}R_{\text{calculated}}}{^{31}R_{\text{measured}}} - 1 \tag{27}$$

where $^{31}R_{\text{calculated}}$ is calculated by plugging the least squares γ and κ into eqn. (10), and $^{31}R_{\text{measured}}$ represents the measured ^{31}R for each reference material. In the intercalibration exercise, the mean of the absolute values of $^{31}\delta^{\text{error}}$ from least squares γ and κ solutions ranged from 0.27 ‰ to 0.86 ‰ (Table S2), similar in magnitude to the $^{31}\delta$ analytical uncertainty for Labs 1 and 2 (Table S5). This indicates that the amount of error introduced by using the least squares optimization is similar to the measurement error in $^{31}\delta$ (Table S2, Table S5). In comparison, the $^{3}\delta^{\text{error}}$ introduced by the algebraic solution corresponded to values of ($^{31}R_{\text{calculated}}$ − $^{31}R_{\text{measured}}$) within machine precision (Table S2).

4.3 Variability in fragmentation behavior

As shown above, $\gamma - \kappa$, as opposed to the individual values of γ and κ, is the best constrained parameter in the scrambling calculation. We show below that $\gamma - \kappa$ also has the greatest impact on $\delta(^{15}N^\alpha)$, $\delta(^{15}N^\beta)$, and $\delta(^{15}N^{sp})$. $\gamma - \kappa$ is proportional to $^{31}\delta - {}^{45}\delta$, and thus is a metric of an instrument's scrambling behavior.

To examine the change in the fragmentation behavior of a single IRMS over time, we compiled values of $\gamma - \kappa$ for Lab 1 from June 2018 – March 2021 (Figure 3). To equally weigh each day of running the instrument, first, we calculated a daily mean $\gamma - \kappa$, then calculated a five-day running average of $\gamma - \kappa$ from these daily means. The value of $\gamma - \kappa$ varied throughout the time series, with a mean of 0.092±0.002. High volatility in $\gamma - \kappa$ in February-April 2019 corresponded with a period when the lab temperature was poorly controlled, with strong day-night variation (Figure 3). During periods when the lab temperature was stable, $\gamma - \kappa$ tended to increase as the instrument box and trap currents diverged with filament age, although no linear relationship emerged.

There are several reasons why the scrambling behavior of the ion source might change over time, as well as differing between instruments. The NO^+ fragment ion can be produced by one of several routes from N_2O^+ [75,76]. The pathways and associated isotope effects for the formation of fragment ions are affected by collision frequency, the distribution of excited states, and the time spent in the ion source, which suggests that ion source conditions such as vapor pressure, ionizing energy, and accelerating voltage may all influence the fragmentation behavior of an IRMS system[54,75–78]. Future work could track the effect of variation in these parameters on the fragmentation behavior of the instrument, as in Westley et al.[54], which may allow for optimization of fragmentation and scrambling in the ion source.

For these reasons, performing the scrambling calibration only once is insufficient to obtain high-quality N_2O isotopocule data. Instead, it is important to recalibrate an IRMS system for scrambling on a regular basis since ion source conditions may change with time and can shift abruptly with events such as filament changes. We recommend using a running average of γ and κ over a window corresponding to 10 pairings of reference materials, corresponding to a five-day window if two pairs of reference materials are run per day. If there is high volatility in γ and κ, as seen above in March-April 2019, it may be necessary to shorten this window, to apply scrambling corrections most appropriate to instrument conditions.

4.4 Sensitivity of position-dependent δ values to uncertainty in scrambling coefficients

pyisotopomer

561 The uncertainty in $\delta(^{15}N^{\alpha})$, $\delta(^{15}N^{\beta})$, and $\delta(^{15}N^{sp})$ associated with the uncertainty in each
562 scrambling coefficient is less straightforward to assess than the uncertainty in ^{31}R given by eqns.
563 (23) and (24), due to the nonlinear relationship between $\delta(^{15}N^{\alpha})$, $\delta(^{15}N^{\beta})$, γ, and κ. (see eqn. (53)
564 of Kaiser and Röckmann, 2008). A first order approximation of $\delta(^{15}N^{sp})$ is given by
565 (supplementary text S4):

$$\delta(^{15}N^{sp}) \approx \frac{2(1 - \gamma + \kappa)}{1 - \gamma - \kappa}\left(^{31}\delta - {}^{45}\delta\right) \tag{28}$$

566 From this equation, it is apparent that $\delta(^{15}N^{sp})$ is modulated primarily by the difference γ
567 $- \kappa$, rather than the individual values of γ and κ. It is also apparent that $\gamma - \kappa$ is proportional to $^{31}\delta$
568 $- {}^{45}\delta$.
569 A Monte Carlo simulation can be a useful way of visualizing how γ, κ, and, $\gamma - \kappa$ impact
570 $\delta(^{15}N^{\alpha})$, $\delta(^{15}N^{\beta})$, and $\delta(^{15}N^{sp})$. We performed two sensitivity experiments with data from Lab 1:
571   1) sensitivity of $\delta(^{15}N^{\alpha})$, $\delta(^{15}N^{\beta})$, and $\delta(^{15}N^{sp})$ to $\gamma - \kappa$;
572   2) sensitivity of $\delta(^{15}N^{\alpha})$, $\delta(^{15}N^{\beta})$, and $\delta(^{15}N^{sp})$ to the individual values of γ and κ, holding
573   their difference constant.
574 For the first sensitivity experiment, a Monte Carlo simulation was used to introduce
575 random uncertainty in the γ and κ values used to calculate δ values of three reference materials.
576 Based on Table S2, we chose $\gamma = 0.174$ and $\kappa = 0.083$ as central values and varied $\gamma - \kappa$ such that
577 the standard deviation of $\gamma - \kappa$ was equal to 10 % of the mean (0.091). For the second sensitivity
578 experiment, we modeled γ and κ in tandem as random numbers centered around $\gamma = 0.174$ and $\kappa =$
579 0.083, with uncertainties equal to 10 % of the mean γ, and held $\gamma - \kappa$ constant at 0.091. For both
580 experiments, we sampled 1000 pairs of γ and κ, and then calculated the 1000 simulated values of
581 $\delta(^{15}N^{\alpha})$, $\delta(^{15}N^{\beta})$, and $\delta(^{15}N^{sp})$ for the three reference materials (CA06261, 53504, CA08214).
582 This analysis showed that a 10 % relative uncertainty in $\gamma - \kappa$ can lead to large variations
583 in $\delta(^{15}N^{\alpha})$, $\delta(^{15}N^{\beta})$, and $\delta(^{15}N^{sp})$, e.g., pooled standard deviations of 17.1-18.5 ‰ for $\delta(^{15}N^{sp})$
584 (Figure 4a-c). In contrast, a 10 % relative error in γ, keeping $\gamma - \kappa$ constant, led to pooled
585 standard deviations of 1.0-4.3 ‰ in $\delta(^{15}N^{sp})$ (Figure 4d-f). In both experiments, varying γ and κ
586 produced the most variability for reference material 53504, whose $\delta(^{15}N^{sp})$ was greatest in
587 magnitude.
588 These results reflect the earlier conclusion that $\gamma - \kappa$ is the best constrained parameter in
589 the scrambling calculation, and, conversely, that this difference has the greatest effect on
590 $\delta(^{15}N^{sp})$. Thus, we recommend regular scrambling calibrations, as assuming the wrong $\gamma - \kappa$
591 difference may have a significant impact on site preferences calculated from these coefficients.
592
593 **4.5 Comparison of results between two IRMS laboratories**
594 The application of pyisotopomer was tested through an intercalibration including four
595 reference materials and two Lake Lugano samples measured by two IRMS laboratories, plus two
596 additional reference materials run in Lab 1. Using an average γ and κ produced by the algebraic
597 method from the pairing of reference materials 53504 and CA08214, isotopomers were
598 calculated for lake water unknowns, four reference materials run as unknowns for quality
599 control, and the two reference materials used in the calibration and (Table 2). This exercise was
600 repeated, calculating γ and κ instead with least squares method and the pairing of reference
601 materials CA06261 and CA08214 (Table S4). The root mean square deviation (RMSD) for each
602 reference material was calculated by comparison to the calibrated values provided by a previous
603 intercalibration effort[56] (for atmosphere-equilibrated seawater), an internal standard (B6), and
604 four gases sourced from J. Mohn (S2, CA06261, 53504, and CA08214). Almost all isotopomer

605   values produced by the least squares optimization (Table S4) were within error of those produced
606   by the algebraic solution (Table 2); the latter is discussed below.
607   The $\delta(^{15}N^{bulk})$ measured by the two labs displayed good agreement for each of the four
608   reference materials, as well as the lake water samples. The $\delta(^{15}N^{bulk})$ RMSDs ranged from 0.2 to
609   0.6 ‰ (Table 2), all of which were smaller than the 0.8 ‰ presented for IRMS labs by Mohn et
610   al., 2014). The RMSD for atmospheric N_2O was highest, at 0.6 ‰. For both lake water samples,
611   the $\delta(^{15}N^{bulk})$ values measured by Lab 1 and Lab 2 were statistically indistinguishable (Table 2;
612   Figure S4). Likewise, the $\delta(^{18}O)$ measured by the two labs displayed good agreement for each of
613   the four reference materials measured by both labs, as well as the lake water samples. The $\delta(^{18}O)$
614   RMSDs were slightly greater than the 1.00 ‰ presented for IRMS labs by Mohn et al. (2014),
615   ranging from 0.5 ‰–1.7 ‰, with the greatest RMSD for reference material 53504 (Table 2). For
616   the lake water unknowns, the $\delta(^{18}O)$ values measured by the two labs were within error of each
617   other (Table 2; Figure S4).
618   The $\delta(^{15}N^{\alpha})$ measured by the two labs also showed good agreement for reference
619   materials CA06261, CA08214, and atmosphere-equilibrated seawater: in each case, the
620   combined RMSD was less than 2.4 ‰ (Table 2). This is similar to the data presented in Mohn et
621   al. (2014), who find an RMSD for $\delta(^{15}N^{\alpha})$ for IRMS laboratories of 2.47 ‰. The $\delta(^{15}N^{\alpha})$
622   measured by Lab 1 for reference material 53504 (0.0±1.0 ‰) was lower than both the calibrated
623   value (1.71 ‰) and the value measured by Lab 2 (1.7±1.0 ‰). The values of $\delta(^{15}N^{\alpha})$ measured
624   by the two labs for the two lake water samples, however, were within error of each other. For
625     $\delta(^{15}N^{\beta})$, the RMSDs for each reference material were of a similar order of magnitude to $\delta(^{15}N^{\alpha})$,
626   ranging from 0.2 ‰-2.1 ‰, similar to the value 2.12 ‰ reported by Mohn et al. (2014). The
627     $\delta(^{15}N^{\beta})$ measured by Lab 1 for the lake water unknowns was within error of that measured by
628   Lab 2 (Table 2; Figure S4). Of note, the $\delta(^{15}N^{\beta})$ for the lake water unknown taken at 90 m depth
629   was –32.8 ‰ (average of measurements by Lab 1 and Lab 2), which is far more negative than
630   most values observed previously[26,31].
631   The $\delta(^{15}N^{sp})$ values measured by the two laboratories showed larger standard deviations
632   than the $\delta(^{15}N^{\alpha})$ and $\delta(^{15}N^{\beta})$ individually, which is to be expected, since $\delta(^{15}N^{sp})$ is a measure of
633   difference between the latter two parameters. The $\delta(^{15}N^{sp})$ RMSD values, however, were all less
634   than 3 ‰ for atmosphere-equilibrated seawater, 53504, and CA08214 (Table 2). This represents
635   an improvement on Mohn et al. (2014), who find an RMSD of 4.29 ‰ for $\delta(^{15}N^{sp})$ measured by
636   IRMS laboratories. The $\delta(^{15}N^{sp})$ RMSD for reference material CA06261 was greater, at 4.4 ‰,
637   which may result from this reference material having a more negative $\delta(^{15}N^{\alpha})$ than either of the
638   two reference materials used in the scrambling calibration. The lake water samples showed larger
639   offsets in $\delta(^{15}N^{sp})$ than the reference materials (Figure S4). The lake water sample from 10 m
640   depth showed an especially large difference in $\delta(^{15}N^{sp})$ between Lab 1 and Lab 2: Lab 1
641   measured a mean $\delta(^{15}N^{sp})$ of (18.8±1.6) ‰ at this depth, while Lab 2 measured a mean $\delta(^{15}N^{sp})$
642   of (21.4±2.5) ‰ (Table 2). At 90 m depth, Lab 1 measured a mean $\delta(^{15}N^{sp})$ of 52.3±1.2 ‰, and
643   Lab 2 measured a mean $\delta(^{15}N^{sp})$ of (50.9±0.5) ‰.
644   After size correction and scale normalization, the only consistent difference between
645   measurements made by the two labs were differences in peak area, which may reflect differences
646   in the setup of the purge and trap system and/or differences in instrument sensitivity. The N_2O
647   amounts (in nmol) measured in the lake water samples were also similar between the two labs
648   involved in the intercalibration exercise, indicating that this difference in sensitivity was
649   adequately compensated for by the peak area to amount conversion factor. In the sample taken at
650   10 m depth, Lab 1 found (2.97±0.04) nmol; Lab 2 found (2.31±0.09) nmol. At 90 m depth, Lab 1

651   found (20.46±0.37) nmol; Lab 2 found (19.82±0.01) nmol N_2O. The intercalibration is expressed
652   in terms of N_2O amounts instead of concentrations to eliminate uncertainties in sample volume;
653   all bottle volumes were the same. Thus, we conclude that differences in sample pretreatment
654   procedure were corrected for by the size correction and scale normalization steps, leaving no
655   residual effect on the final δ values or N_2O amounts.
656
657   **4.6 Additional considerations**
658   The pyisotopomer package produces good results if each of the data preprocessing steps
659   properly account for size- and delta-dependent effects on the measured isotope ratios $^{31}\delta$, $^{45}\delta$, and
660   $^{46}\delta$. However, it will produce spurious results under the following circumstances. Firstly, varying
661   blanks may introduce errors due to the size correction not being applicable to samples and
662   reference materials alike. Second, if the $^{45}\delta$ and $^{46}\delta$ scale normalization slope and intercept differ
663   substantially from one and zero (such as a negative slope), there likely exists an issue with the
664   scale normalization (such as the reference materials not spanning a wide enough range in $^{45}\delta$ and
665   $^{46}\delta$). A spurious scale normalization will likewise produce errors in the final isotopocule values.
666   Thirdly, if reference materials that are too close in their site preferences are used to determine γ
667   and κ with the algebraic solution, the resulting coefficients may represent "unphysical" values
668   (i.e., not between 0 and 1); these, however, would be inconsequential if the unknown samples
669   have $\delta(^{15}N^{sp})$ values close to these reference materials. Finally, $\delta(^{17}O)$ is calculated from a mass
670   dependent relationship with $\delta(^{18}O)$ (the parameters of which can be adjusted with keyword
671   arguments to the Scrambling and Isotopomers functions) unless $\Delta(^{17}O)$ is determined
672   separately[60,62,63] and entered in the data corrections template.
673
674   **5. Conclusion: How to obtain high-quality N_2O isotopocule data using pyisotopomer**
675   Using pyisotopomer and three reference materials, one can characterize the scrambling
676   behavior for a given IRMS and apply those scrambling coefficients to calculate the isotopocule
677   values of unknown samples. To ensure high-quality results from these calculations, we provide
678   the following recommendations. Firstly, if reference materials with suitably distinct site
679   preferences are available, we recommend calculating the scrambling coefficients γ and κ from
680   algebraic solution of eqns. (11) and (12), which is the default method in the Scrambling function
681   of pyisotopomer. We offer the least squares approach as an alternative, with the following
682   caveats: 1) The least squares solver finds a minimum close to the initial guess for γ and κ. As
683   such, if the solver is fed an initial guess other than the absolute minimum calculated from the
684   algebraic solution, it will find the "wrong" absolute value of γ and κ. It will, however, find the
685   correct value of $\gamma - \kappa$, which has a much larger impact on calculated isotopocules. 2) Using the
686   "wrong" scrambling coefficients will have only a small effect if the unknowns are close in their
687   $\delta(^{15}N^{\alpha})$, $\delta(^{15}N^{\beta})$, and $\delta(^{15}N^{sp})$ to those of the reference materials but will have a deleterious effect
688   as the unknowns diverge in their isotopomer values from the reference materials. 3) If an initial
689   guess is available, such as through a calibration with the algebraic solution, this should be used
690   as the initial guess for the least squares solver. Otherwise, we recommend iterating through the
691   scrambling calculation twice, using the solution from the first iteration as the initial guess for
692   subsequent calculations. It is necessary to run paired reference materials daily to obtain accurate
693   running estimates of γ and κ. It is recommended to convert these daily estimates to a one-week
694   running average and use that average to calculate the isotopocules of unknown samples.
695   Using pyisotopomer in an intercalibration exercise and implementing the above
696   recommendations, we find good agreement between the calibrated δ values measured by two

different IRMS labs for both reference materials and natural lake samples. We conclude that while the intercalibration results demonstrate potential for further improvement in precision, the intercalibration of $\delta(^{15}N^{sp})$ using a uniform scrambling calculation (pyisotopomer) presented here represents an improvement upon previous N_2O intercalibrations.

In this paper, we demonstrate the need to support efforts to generate and distribute reference gases to the community. At present, the only commercially available reference materials are USGS 51 and USGS 52[55], which do not have sufficiently distinct values of $\delta(^{15}N^{sp})$ to obtain precise values of γ and κ with the algebraic solution unless the user is able to achieve extremely small measurement uncertainties in ^{31}R. There have been other efforts to produce more calibrated N_2O reference gases[79], but these gases are not yet commercially available. A fully funded program is needed to produce reference materials such as 53504, which — combined with reference materials such as USGS 51 and USGS 52 — should provide users with precise and accurate N_2O isotopocule calibrations.

Data availability statement

References

1. Yung YL, Wang WC, Lacis AA. Greenhouse effect due to atmospheric nitrous oxide. *Geophys Res Lett*. 1976;3(10):619-621. doi:10.1029/GL003i010p00619

2. Smith C, Nicholls ZRJ, Armour K, et al. The Earth's Energy Budget, Climate Feedbacks, and Climate Sensitivity Supplementary Material. In: Masson-Delmotte V, Zhai P, Pirani A, et al., eds. *Climate Change 2021: The Physical Science Basis. Contribution of Working Group I to the Sixth Assessment Report of the Intergovernmental Panel on Climate Change*. Cambridge University Press; 2021. Accessed October 4, 2021. https://www.ipcc.ch/report/ar6/wg1/downloads/report/IPCC_AR6_WGI_Chapter_07_Supplementary_Material.pdf

3. Crutzen PJ. The influence of nitrogen oxides on the atmospheric ozone content. *Q J R Meteorol Soc*. 1970;96(408):320-325. doi:10.1002/qj.49709640815

4. Ravishankara AR, Daniel JS, Portmann RW. Nitrous Oxide (N2O): The Dominant Ozone-Depleting Substance Emitted in the 21st Century. *Science*. 2009;326(5949):123-125. doi:10.1126/science.1176985

5. Wuebbles DJ. Nitrous Oxide: No Laughing Matter. *Science*. 2009;326(5949):56-57. doi:10.1126/science.1179571

6. Müller R. The impact of the rise in atmospheric nitrous oxide on stratospheric ozone. *Ambio*. 2021;50(1):35-39. doi:10.1007/s13280-020-01428-3

7. Kim KR, Craig H. Nitrogen-15 and Oxygen-18 Characteristics of Nitrous Oxide: A Global Perspective. *Science*. 1993;262(5141):1855-1857. doi:10.1126/science.262.5141.1855

8. Pérez T, Trumbore SE, Tyler SC, Davidson EA, Keller M, Camargo PB de. Isotopic variability of N2O emissions from tropical forest soils. *Glob Biogeochem Cycles*. 2000;14(2):525-535. doi:10.1029/1999GB001181

9. Kim KR, Craig H. Two-isotope characterization of N20 in the Pacific Ocean and constraints on its origin in deep water. *Nature*. 1990;347(6288):58-61. doi:10.1038/347058a0

10. Dore JE, Popp BN, Karl DM, Sansone FJ. A large source of atmospheric nitrous oxide from subtropical North Pacific surface waters. *Nature*. 1998;396(6706):63-66. doi:10.1038/23921

11. Naqvi SWA, Naik H, Jayakumar A, et al. Seasonal Anoxia Over the Western Indian Continental Shelf. In: Wiggert JD, Hood RR, Naqvi SWA, Brink KH, Smith SL, eds. *Geophysical Monograph Series*. Vol 185. American Geophysical Union; 2009:333-345. doi:10.1029/2008GM000745

12. Yoshida N, Hattori A, Saino T, Matsuo S, Wada E. 15N/14N ratio of dissolved N2O in the eastern tropical Pacific Ocean. *Nature*. Published online 1984. doi:10.1038/307442A0

755   13.   Rahn T, Wahlen M. Stable Isotope Enrichment in Stratospheric Nitrous Oxide. *Science*.
756   1997;278(5344):1776-1778. doi:10.1126/science.278.5344.1776

757   14.   Rahn T, Wahlen M. A reassessment of the global isotopic budget of atmospheric nitrous
758   oxide. *Glob Biogeochem Cycles*. 2000;14(2):537-543. doi:10.1029/1999GB900070

759   15.   Yoshida N. 15N-depleted N2O as a product of nitrification. *Nature*. 1988;335(6190):528-
760   529. doi:10.1038/335528a0

761   16.   Barford CC, Montoya JP, Altabet MA, Mitchell R. Steady-State Nitrogen Isotope Effects of
762   N2 and N2O Production in Paracoccus denitrificans. *Appl Environ Microbiol*.
763   1999;65(3):989-994. doi:10.1128/AEM.65.3.989-994.1999

764   17.   Pérez T, Trumbore SE, Tyler SC, et al. Identifying the agricultural imprint on the global
765   N2O budget using stable isotopes. *J Geophys Res Atmospheres*. 2001;106(D9):9869-9878.
766   doi:10.1029/2000JD900809

767   18.   Yamulki S, Toyoda S, Yoshida N, Veldkamp E, Grant B, Bol R. Diurnal fluxes and the
768   isotopomer ratios of N2O in a temperate grassland following urine amendment. *Rapid
769   Commun Mass Spectrom*. 2001;15(15):1263-1269. doi:10.1002/rcm.352

770   19.   Lewicka-Szczebak D, Augustin J, Giesemann A, Well R. Quantifying N2O reduction to N2
771   based on N2O isotopocules – validation with independent methods (helium incubation and
772   15N gas flux method). *Biogeosciences*. 2017;14(3):711-732. doi:https://doi.org/10.5194/bg-
773   14-711-2017

774   20.   Verhoeven E, Barthel M, Yu L, et al. Early season N_2O emissions under variable water
775   management in rice systems: source-partitioning emissions using isotope ratios along a
776   depth profile. *Biogeosciences*. 2019;16(2):383-408. doi:https://doi.org/10.5194/bg-16-383-
777   2019

778   21.   Yoshida N, Toyoda S. Constraining the atmospheric N2O budget from intramolecular site
779   preference in N2O isotopomers. *Nature*. 2000;405(6784):330-334. doi:10.1038/35012558

780   22.   Prokopiou M, Martinerie P, Link to external site this link will open in a new window, et al.
781   Constraining N2O emissions since 1940 using firn air isotope measurements in both
782   hemispheres. *Atmospheric Chem Phys*. 2017;17(7):4539-4564. doi:10.5194/acp-17-4539-
783   2017

784   23.   Yu L, Harris E, Henne S, et al. The isotopic composition of atmospheric nitrous oxide
785   observed at the high-altitude research station Jungfraujoch, Switzerland. *Atmospheric Chem
786   Phys*. 2020;20(11):6495-6519. doi:10.5194/acp-20-6495-2020

787   24.   Toyoda S, Yoshida N, Miwa T, et al. Production mechanism and global budget of N2O
788   inferred from its isotopomers in the western North Pacific. *Geophys Res Lett*. 2002;29(3):7-
789   1-7-4. doi:10.1029/2001GL014311

790   25.   Popp BN, Westley MB, Toyoda S, et al. Nitrogen and oxygen isotopomeric constraints on
791   the origins and sea-to-air flux of N2O in the oligotrophic subtropical North Pacific gyre.
792   *Glob Biogeochem Cycles*. 2002;16(4):12-1-12-10. doi:10.1029/2001GB001806

793   26.   Yamagishi H, Westley MB, Popp BN, et al. Role of nitrification and denitrification on the
794   nitrous oxide cycle in the eastern tropical North Pacific and Gulf of California. *J Geophys
795   Res Biogeosciences*. 2007;112(G2). doi:10.1029/2006JG000227

796   27.   Yamagishi H, Yoshida N, Toyoda S, Popp BN, Westley MB, Watanabe S. Contributions of
797   denitrification and mixing on the distribution of nitrous oxide in the North Pacific. *Geophys
798   Res Lett*. 2005;32(4). doi:10.1029/2004GL021458

799   28.   Westley MB, Yamagishi H, Popp BN, Yoshida N. Nitrous oxide cycling in the Black Sea
800   inferred from stable isotope and isotopomer distributions. *Deep Sea Res Part II Top Stud
801   Oceanogr*. 2006;53(17-19):1802-1816. doi:10.1016/j.dsr2.2006.03.012

802   29.   Farías L, Castro-González M, Cornejo M, et al. Denitrification and nitrous oxide cycling
803   within the upper oxycline of the eastern tropical South Pacific oxygen minimum zone.
804   *Limnol Oceanogr*. 2009;54(1):132-144. doi:10.4319/lo.2009.54.1.0132

805   30.   Casciotti KL, Forbes M, Vedamati J, Peters BD, Martin TS, Mordy CW. Nitrous oxide
806   cycling in the Eastern Tropical South Pacific as inferred from isotopic and isotopomeric
807   data. *Deep Sea Res Part II Top Stud Oceanogr*. 2018;156:155-167.
808   doi:10.1016/j.dsr2.2018.07.014

809   31.   Bourbonnais A, Letscher RT, Bange HW, et al. N2O production and consumption from
810   stable isotopic and concentration data in the Peruvian coastal upwelling system. *Glob
811   Biogeochem Cycles*. 2017;31(4):678-698. doi:10.1002/2016GB005567

812   32.   Toyoda S, Yoshida O, Yamagishi H, Fujii A, Yoshida N, Watanabe S. Identifying the
813   origin of nitrous oxide dissolved in deep ocean by concentration and isotopocule analyses.
814   *Sci Rep*. 2019;9(1):1-9. doi:10.1038/s41598-019-44224-0

815   33.   Kelly CL, Travis NM, Baya PA, Casciotti KL. Quantifying Nitrous Oxide Cycling Regimes
816   in the Eastern Tropical North Pacific Ocean With Isotopomer Analysis. *Glob Biogeochem
817   Cycles*. 2021;35(2):e2020GB006637. doi:10.1029/2020GB006637

818   34.   Toyoda S, Kakimoto T, Kudo K, et al. Distribution and Production Mechanisms of N2O in
819   the Western Arctic Ocean. *Glob Biogeochem Cycles*. 2021;35(4):e2020GB006881.
820   doi:https://doi.org/10.1029/2020GB006881

821   35.   Friedman L, Bigeleisen J. Oxygen and Nitrogen Isotope Effects in the Decomposition of
822   Ammonium Nitrate. *J Chem Phys*. 1950;18(10):1325-1331. doi:10.1063/1.1747471

823   36.   Toyoda S, Yoshida N. Determination of nitrogen isotopomers of nitrous oxide on a
824   modified isotope ratio mass spectrometer. *Anal Chem*. 1999;71(20):4711-4718.
825   doi:10.1021/ac9904563

826   37. Brenninkmeijer CAM, Röckmann T. Mass spectrometry of the intramolecular nitrogen
827   isotope distribution of environmental nitrous oxide using fragment-ion analysis. *Rapid*
828   *Commun Mass Spectrom*. 1999;13(20):2028-2033. doi:10.1002/(SICI)1097-
829   0231(19991030)13:20<2028::AID-RCM751>3.0.CO;2-J

830   38. Kaiser J, Brenninkmeijer CAM, Röckmann T. Intramolecular 15N and 18O fractionation in
831   the reaction of N2O with O(1D) and its implications for the stratospheric N2O isotope
832   signature. *J Geophys Res Atmospheres*. 2002;107(D14):ACH 16-1-ACH 16-14.
833   doi:10.1029/2001JD001506

834   39. Kaiser J. *Stable Isotope Investigations of Atmospheric Nitrous Oxide*. Johannes Gutenberg
835   University of Mainz; 2003. https://doi.org/10.25358/openscience-3976

836   40. Röckmann T, Levin I. High-precision determination of the changing isotopic composition
837   of atmospheric N2O from 1990 to 2002. *J Geophys Res Atmospheres*. 2005;110(D21).
838   doi:10.1029/2005JD006066

839   41. Yung YL, Miller CE. Isotopic Fractionation of Stratospheric Nitrous Oxide. *Science*.
840   1997;278(5344):1778-1780. doi:10.1126/science.278.5344.1778

841   42. Röckmann T, Kaiser J, Brenninkmeijer CAM, et al. Isotopic enrichment of nitrous oxide
842   (15N14NO, 14N15NO, 14N14N18O) in the stratosphere and in the laboratory. *J Geophys*
843   *Res Atmospheres*. 2001;106(D10):10403-10410. doi:10.1029/2000JD900822

844   43. Toyoda S, Yoshida N, Urabe T, et al. Temporal and latitudinal distributions of stratospheric
845   N2O isotopomers. *J Geophys Res Atmospheres*. 2004;109(D8). doi:10.1029/2003JD004316

846   44. Kaiser J, Engel A, Borchers R, Rockmann T. Probing stratospheric transport and chemistry
847   with new balloon and aircraft observations of the meridional and vertical N2O isotope
848   distribution. *Atmos Chem Phys*. Published online 2006:22.

849   45. Park S, Atlas EL, Boering KA. Measurements of N2O isotopologues in the stratosphere:
850   Influence of transport on the apparent enrichment factors and the isotopologue fluxes to the
851   troposphere. *J Geophys Res Atmospheres*. 2004;109(D1). doi:10.1029/2003JD003731

852   46. Sutka RL, Ostrom NE, Ostrom PH, Gandhi H, Breznak JA. Nitrogen isotopomer site
853   preference of N2O produced by Nitrosomonas europaea and Methylococcus capsulatus
854   Bath. *Rapid Commun Mass Spectrom RCM*. 2003;17(7):738-745. doi:10.1002/rcm.968

855   47. Sutka RL, Ostrom NE, Ostrom PH, et al. Distinguishing Nitrous Oxide Production from
856   Nitrification and Denitrification on the Basis of Isotopomer Abundances. *Appl Environ*
857   *Microbiol*. 2006;72(1):638-644. doi:10.1128/AEM.72.1.638-644.2006

858   48. Sutka RL, Ostrom NE, Ostrom PH, Gandhi H, Breznak JA. Nitrogen isotopomer site
859   preference of N2O produced by Nitrosomonas europaea and Methylococcus capsulatus
860   Bath. *Rapid Commun Mass Spectrom*. 2004;18(12):1411-1412. doi:10.1002/rcm.1482

861   49.   Toyoda S, Mutobe H, Yamagishi H, Yoshida N, Tanji Y. Fractionation of N2O isotopomers
862   during production by denitrifier. *Soil Biol Biochem*. 2005;37(8):1535-1545.
863   doi:10.1016/j.soilbio.2005.01.009

864   50.   Frame CH, Casciotti KL. Biogeochemical controls and isotopic signatures of nitrous oxide
865   production by a marine ammonia-oxidizing bacterium. *Biogeosciences*. 2010;7(9):2695-
866   2709. doi:10.5194/bg-7-2695-2010

867   51.   Lazo-Murphy BM, Larson S, Staines S, et al. Nitrous oxide production and isotopomer
868   composition by fungi isolated from salt marsh sediments. *Front Mar Sci*. 2022;9. Accessed
869   January 3, 2023. https://www.frontiersin.org/articles/10.3389/fmars.2022.1098508

870   52.   Ostrom NE, Pitt A, Sutka R, et al. Isotopologue effects during N2O reduction in soils and in
871   pure cultures of denitrifiers. *J Geophys Res Biogeosciences*. 2007;112(G2).
872   doi:10.1029/2006JG000287

873   53.   Kaiser J, Park S, Boering KA, Brenninkmeijer CAM, Hilkert A, Röckmann T. Mass
874   spectrometric method for the absolute calibration of the intramolecular nitrogen isotope
875   distribution in nitrous oxide. *Anal Bioanal Chem*. 2004;378(2):256-269.
876   doi:10.1007/s00216-003-2233-2

877   54.   Westley MB, Popp BN, Rust TM. The calibration of the intramolecular nitrogen isotope
878   distribution in nitrous oxide measured by isotope ratio mass spectrometry. *Rapid Commun
879   Mass Spectrom*. 2007;21(3):391-405. doi:10.1002/rcm.2828

880   55.   Ostrom NE, Gandhi H, Coplen TB, et al. Preliminary assessment of stable nitrogen and
881   oxygen isotopic composition of USGS51 and USGS52 nitrous oxide reference gases and
882   perspectives on calibration needs. *Rapid Commun Mass Spectrom*. 2018;32(15):1207-1214.
883   doi:10.1002/rcm.8157

884   56.   Mohn J, Wolf B, Toyoda S, et al. Interlaboratory assessment of nitrous oxide isotopomer
885   analysis by isotope ratio mass spectrometry and laser spectroscopy: current status and
886   perspectives. *Rapid Commun Mass Spectrom*. 2014;28(18):1995-2007.
887   doi:10.1002/rcm.6982

888   57.   Kelly CL. pyisotopomer: Nitrous oxide isotopocule data corrections in Python. Published
889   online January 5, 2023. Accessed March 13, 2023. https://pypi.org/project/pyisotopomer/

890   58.   Baertschi P. Absolute18O content of standard mean ocean water. *Earth Planet Sci Lett*.
891   1976;31(3):341-344. doi:10.1016/0012-821X(76)90115-1

892   59.   Jabeen I, Kusakabe M. Determination of δ 17O values of reference water samples VSMOW
893   and SLAP. *Chem Geol*. 1997;143:115-119. doi:10.1016/S0009-2541(97)00109-5

894   60.   Kaiser J, Röckmann T, Brenninkmeijer CAM. Complete and accurate mass spectrometric
895   isotope analysis of tropospheric nitrous oxide. *J Geophys Res Atmospheres*.
896   2003;108(D15). doi:10.1029/2003JD003613

897   61. Kaiser J, Röckmann T. Correction of mass spectrometric isotope ratio measurements for
898   isobaric isotopologues of O2, CO, CO2, N2O and SO2. *Rapid Commun Mass Spectrom*.
899   2008;22(24):3997-4008. doi:10.1002/rcm.3821

900   62. Kaiser J, Hastings MG, Houlton BZ, Röckmann T, Sigman DM. Triple Oxygen Isotope
901   Analysis of Nitrate Using the Denitrifier Method and Thermal Decomposition of N2O.
902   *Anal Chem*. 2007;79(2):599-607. doi:10.1021/ac061022s

903   63. Wankel SD, Ziebis W, Buchwald C, et al. Evidence for fungal and chemodenitrification
904   based N 2 O flux from nitrogen impacted coastal sediments. *Nat Commun*. 2017;8(1):1-11.
905   doi:10.1038/ncomms15595

906   64. Magyar PM, Orphan VJ, Eiler JM. Measurement of rare isotopologues of nitrous oxide by
907   high-resolution multi-collector mass spectrometry. *Rapid Commun Mass Spectrom*.
908   2016;30(17):1923-1940. doi:10.1002/rcm.7671

909   65. Kelly CL. ckelly314/pyisotopomer: v1.0.4. Published online January 19, 2023.
910   doi:10.5281/zenodo.7552724

911   66. McIlvin MR, Casciotti KL. Technical updates to the bacterial method for nitrate isotopic
912   analyses. *Anal Chem*. 2011;83(5):1850-1856. doi:10.1021/ac1028984

913   67. McIlvin MR, Casciotti KL. Fully automated system for stable isotopic analyses of dissolved
914   nitrous oxide at natural abundance levels. *Limnol Oceanogr Methods*. 2010;8(2):54-66.
915   doi:10.4319/lom.2010.8.54

916   68. Scott KM, Lu X, Cavanaugh CM, Liu JS. Optimal methods for estimating kinetic isotope
917   effects from different forms of the Rayleigh distillation equation 1 1Associate editor: J.
918   Horita. *Geochim Cosmochim Acta*. 2004;68(3):433-442. doi:10.1016/S0016-
919   7037(03)00459-9

920   69. LI W. Measurement of the absolute abundance of oxygen-17 in V-SMOW. *Chin Sci Bull*.
921   1988;33:1610-1613. Accessed June 10, 2021. https://ci.nii.ac.jp/naid/80004607415/

922   70. Santoro AE, Buchwald C, McIlvin MR, Casciotti KL. Isotopic Signature of N2O Produced
923   by Marine Ammonia-Oxidizing Archaea. *Science*. 2011;333(6047):1282-1285.
924   doi:10.1126/science.1208239

925   71. Dutton GS, Elkins JW, Hall BD. Nitrous Oxide data from the NOAA/ESRL halocarbons in
926   situ program. Published online 2021. Accessed November 19, 2021.
927   https://data.nodc.noaa.gov/cgi-bin/iso?id=gov.noaa.ncdc:C01556

928   72. Inoue HY, Mook WG. Equilibrium and kinetic nitrogen and oxygen isotope fractionations
929   between dissolved and gaseous N2O. *Chem Geol*. 1994;113(1):135-148. doi:10.1016/0009-
930   2541(94)90009-4

931   73. Röckmann T, Kaiser J, Brenninkmeijer CAM, Brand WA. Gas chromatography/isotope-
932   ratio mass spectrometry method for high-precision position-dependent 15N and 18O

933   measurements of atmospheric nitrous oxide. *Rapid Commun Mass Spectrom*.
934   2003;17(16):1897-1908. doi:10.1002/rcm.1132

935 74. Glover DM, Jenkins WJ, Doney SC. *Modeling Methods for Marine Science*. Cambridge
936   University Press; 2011. doi:10.1017/CBO9780511975721

937 75. Lorquet JC, Cadet C. Excited states of gaseous ions: I. Selection rules in photoelectron
938   spectroscopy and photoionization. The case of N2O+. *Int J Mass Spectrom Ion Phys*.
939   1971;7(3):245-254. doi:10.1016/0020-7381(71)80020-7

940 76. Märk E, Märk TD, Kim YB, Stephan K. Absolute electron impact ionization cross section
941   from threshold up to 180 eV for N2O+e→N2O++2e and the metastable and collision
942   induced dissociation of N2O+. *J Chem Phys*. 1981;75(9):4446-4453. doi:10.1063/1.442611

943 77. Bigeleisen J. Chemistry of Isotopes. *Science*. 1965;147(3657):463-471.
944   doi:10.1126/science.147.3657.463

945 78. Begun GM, Landau L. Metastable Transitions in N2O+. *J Chem Phys*. 1962;36(4):1083-
946   1084. doi:10.1063/1.1732641

947 79. Mohn J, Biasi C, Bodé S, et al. Isotopically characterised N2O reference materials for use
948   as community standards. *Rapid Commun Mass Spectrom*. 2022;36(13):e9296.
949   doi:10.1002/rcm.9296

950
951

Table 1. Reference materials for N₂O isotopic analysis and intercalibration. Except for one internal standard (B6), calibrated values were provided via independent measurement by S. Toyoda, Tokyo Tech., J. Mohn, EMPA; or, in the case of tropospheric N₂O, the 2018 annual average measured at Jungfraujoch, Switzerland, reported by Yu et al. (2020). The laboratories participating in the intercalibration exercise were at Stanford University ("Lab 1") and the University of Basel ("Lab 2"). ^{31}R values represent the inherent, unscrambled ^{31}R of each reference material, calculated from eqn. (6).

Reference material	Matrix	Mole fraction	$\delta(^{15}N^\alpha)$	$\delta(^{15}N^\beta)$	$\delta(^{15}N^{sp})$	$\delta(^{15}N^{bulk})$	$\delta(^{18}O)$	^{31}R $(^{15}R^{\alpha}+^{17}R)$	^{45}R	^{46}R	Calibration by
		µmol mol^{-1}			*(‰, vs. air N₂)*		*(‰, vs. VSMOW)*				
S2 reference gas	Synthetic air	90	5.55	-12.87	18.42	-3.66	32.73	0.004083	0.007712	0.002087	Toyoda & Mohn
B6 reference gas	He	900	-0.40	-0.15	-0.26	-0.28	41.95	0.004063	0.007739	0.002106	Lab 1 internal standard
Tropospheric N₂O (2018 annual average)	Air	~0.33	15.6	-2.3	17.9	6.6	44.4	0.004123	0.007787	0.002111	Yu et al. (2020)
CA06261	Synthetic air	90	-22.21	-49.28	27.07	-35.75	26.94	0.003980	0.007475	0.002075	Toyoda & Mohn
53504	Synthetic air	90	1.71	94.44	-92.73	48.08	36.01	0.004070	0.008093	0.002095	Toyoda & Mohn
CA08214	Synthetic air	90	17.11	-3.43	20.54	6.84	35.39	0.004126	0.007790	0.002093	Toyoda & Mohn
90454	Synthetic air	90	25.73	25.44	0.29	25.59	35.88	0.004158	0.007928	0.002094	Toyoda & Mohn
94321	Synthetic air	90	50.52	2.21	48.31	26.37	35.54	0.004249	0.007934	0.002094	Toyoda & Mohn
Lab 1 pure N₂O direct injection ("A01")	Pure N2O	N/A	0.24	0.12	0.13	0.18	39.85	0.003734	0.007742	0.002101	Toyoda
Lab 2 pure N₂O direct injection	Pure N2O	N/A	-4.07	3.59	-7.66	-0.24	39.25	0.004044	0.007739	0.002100	Mohn

pyisotopomer 27

960 **Table 2.** N_2O isotopic composition of reference materials and two unknowns analyzed by two IRMS laboratories,
961 calculated using γ and κ values determined from reference materials 53504 and CA08214 with the algebraic
962 solution. $\delta(^{15}N^{\alpha})$, $\delta(^{15}N^{\beta})$, $\delta(^{15}N^{sp})$ and $\delta(^{15}N^{bulk})$ are reported in ‰ vs. Air N_2, and $\delta^{18}O$ is reported in ‰ vs.
963 VSMOW. Uncertainties are standard deviations of replicate bottles and do not include calibration uncertainties. The
964 root-mean square deviation (RMSD) was calculated with respect to calibrated values.

965

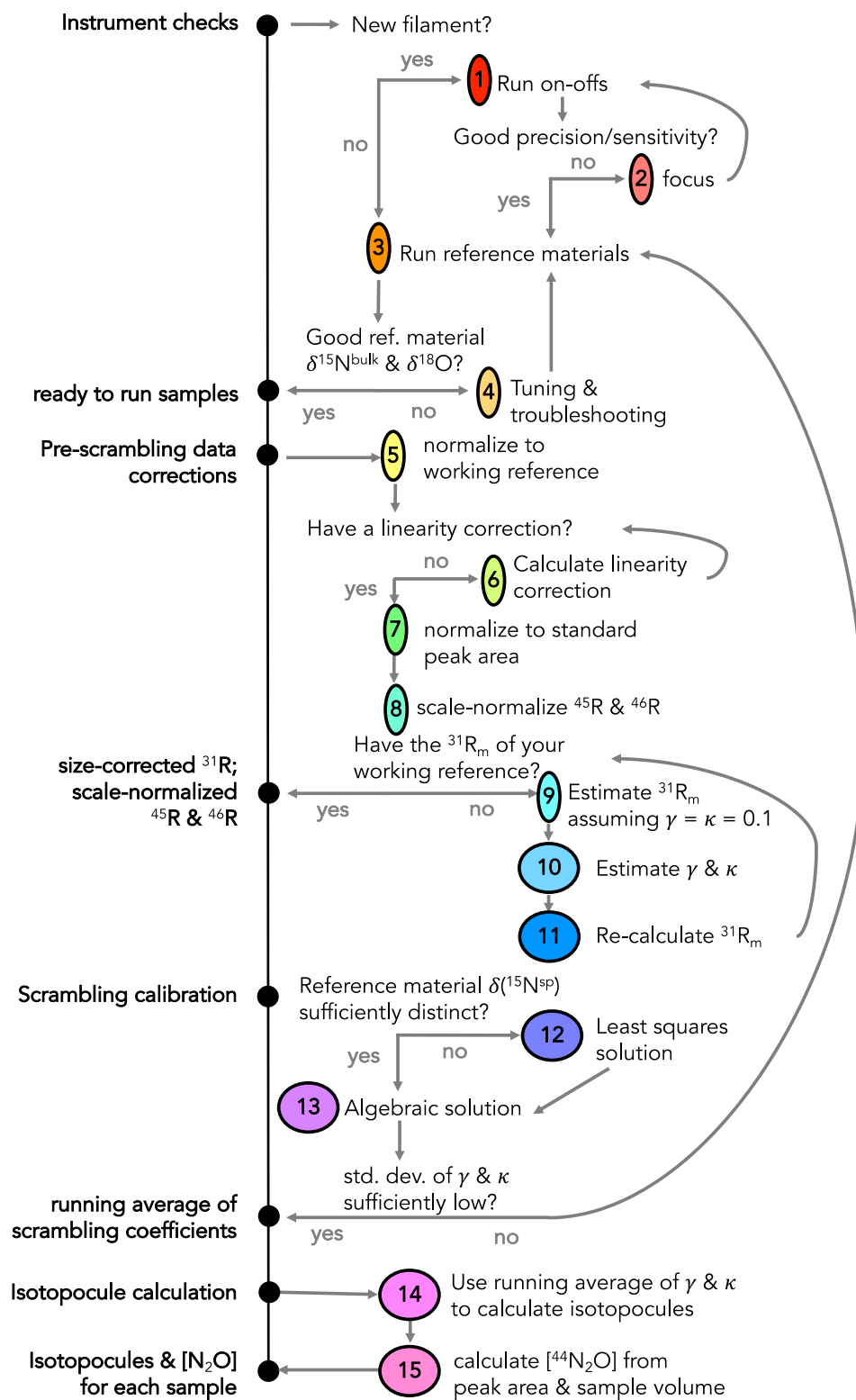| Reference material		n	$\delta(^{15}N^{\alpha})$	σ	$\delta(^{15}N^{\beta})$	σ	$\delta(^{15}N^{sp})$	σ	$\delta(^{15}N^{bulk})$	σ	$\delta(^{18}O)$	σ
					(‰, vs. air N2)						(‰, vs. VSMOW)	
CA06261	Calibrated value		-22.2		-49.3		27.1		-35.7		26.9	
	Lab 1	4	-20.6	1.3	-50.5	1.3	29.9	2.7	-35.6	0.2	28.4	0.8
	Lab 2	16	-20.5	1.4	-50.9	2.6	30.4	3.8	-35.7	1.0	27.6	1.8
	RMSD		2.3		2.1		4.4		0.2		1.5	
53504	Calibrated value		1.7		94.4		-92.7		48.1		36.0	
	Lab 1	4	0.0	1.0	95.7	2.1	-95.7	2.5	47.9	1.1	37.6	0.8
	Lab 2	15	1.7	1.0	94.5	1.9	-92.8	2.9	48.1	0.6	36.4	1.6
	RMSD		1.7		1.3		3.0		0.2		1.7	
CA08214	Calibrated value		17.1		-3.4		20.5		6.8		35.3	
	Lab 1	6	17.0	2.0	-2.4	0.9	19.4	2.9	7.3	0.7	36.3	1.4
	Lab 2	16	17.0	1.1	-3.2	0.7	20.2	1.3	6.9	0.6	36.0	3.6
	RMSD		0.1		1.1		1.2		0.5		1.3	
Tropospheric N_2O	Calibrated value		15.6		-2.3		17.9		6.6		44.4	
	Lab 1	7	15.1	0.8	-2.5	2.3	17.5	2.8	6.3	1.0	43.1	2.1
	Lab 2	2	15.8	1.1	-3.7	0.0	19.5	1.0	6.1	0.5	44.7	1.0
	RMSD		0.6		1.4		1.7		0.6		1.3	
B6	Calibrated value		-0.4		-0.1		-0.3		-0.3		41.9	
	Lab 1	7	-2.2	0.7	1.3	1.0	-3.4	1.2	-0.4	0.7	41.5	1.6
	RMSD		1.8		1.4		3.2		0.2		0.5	
S2	Calibrated value		5.6		-12.9		18.4		-3.7		32.7	
	Lab1	6	5.0	0.5	-13.1	1.6	18.1	1.3	-4.0	1.0	31.5	1.8
	RMSD		0.5		0.2		0.3		0.4		1.2	
Lake Lugano, 10m	Lab 1	3	13.2	0.3	-5.6	1.2	18.8	1.5	3.8	0.4	44.6	1.2
	Lab 2	5	14.8	1.5	-6.6	1.3	21.4	2.5	4.1	0.5	45.5	0.6
Lake Lugano, 90m	Lab 1	3	19.2	0.5	-33.1	0.7	52.3	1.2	-6.9	0.1	56.8	0.1
	Lab 2	2	18.5	0.8	-32.4	0.3	50.9	0.5	-6.9	0.5	55.4	1.9

966

pyisotopomer 28

Figure 1. N₂O data corrections flowchart. Instrument checks, pre-scrambling data corrections, the scrambling calibration, and isotopomer calculations are laid out; numbers in yellow circles correspond to step numbers referred to in the text. Steps 1-4 are performed with raw Isodat output, steps 5-8 are accomplished in the data corrections spreadsheet template, step 9 is a simple calculation, and steps 10-14 are accomplished with the pyisotopomer code.
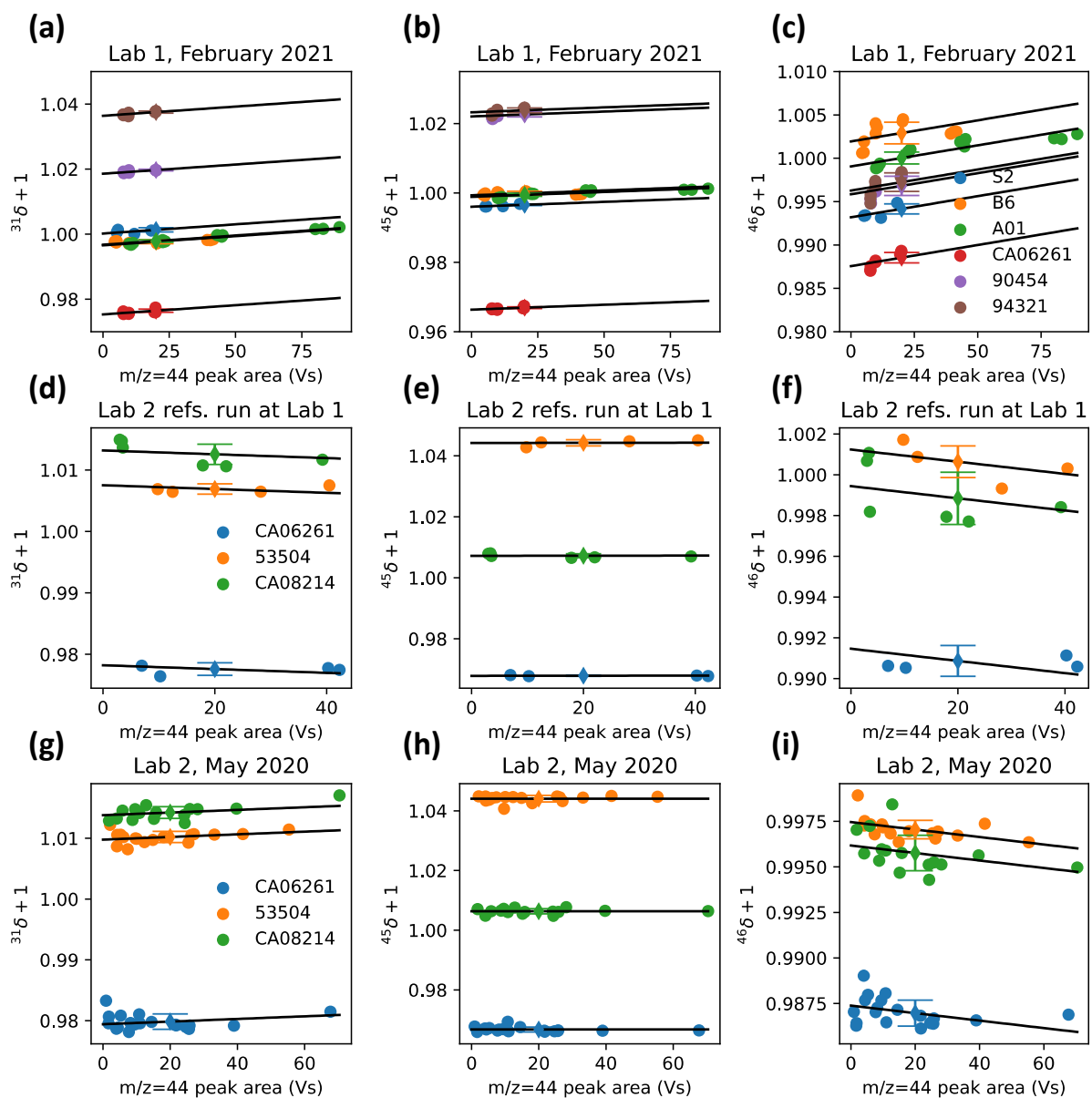
Figure 2. Linearity relations for reference materials used to normalize measured isotope ratios to a peak area of 20 Vs (10 nmol N$_2$O), using the dummy variable method[68]. $^{31}\delta+1$ (a,d,g), $^{45}\delta+1$ (b,e,h), and $^{46}\delta+1$ (c, f, i) are plotted against m/z 44 peak area. Linearity relations are shown for reference materials prepared and run in Lab 1 (a-c), reference materials prepared in Lab 2 but run in Lab 1 (d-f), and reference materials run in Lab 2 (g-i). A common slope (black line) calculated from the dummy variable method for each molecular ion ratio is overlain on each data series (colored circles). The estimated isotope ratio corresponding to a peak area of 20 Vs/10 nmols N$_2$O is also shown for each series (colored diamonds, error bars correspond to the standard error of the predicted y-value).
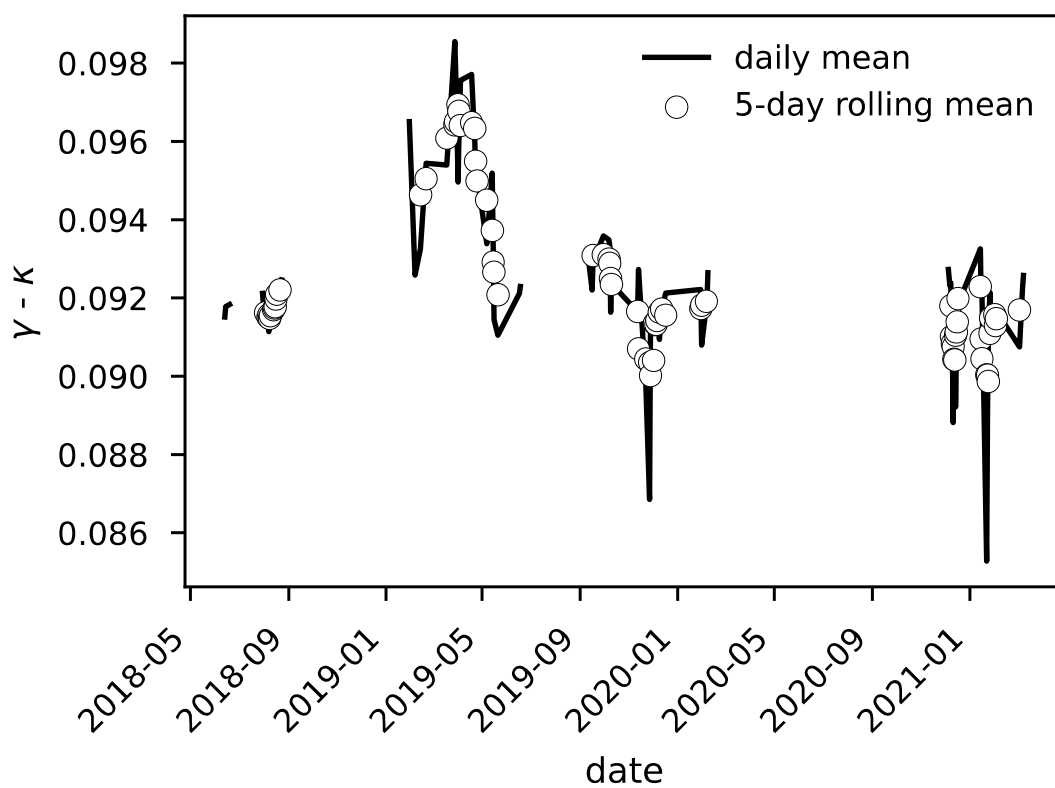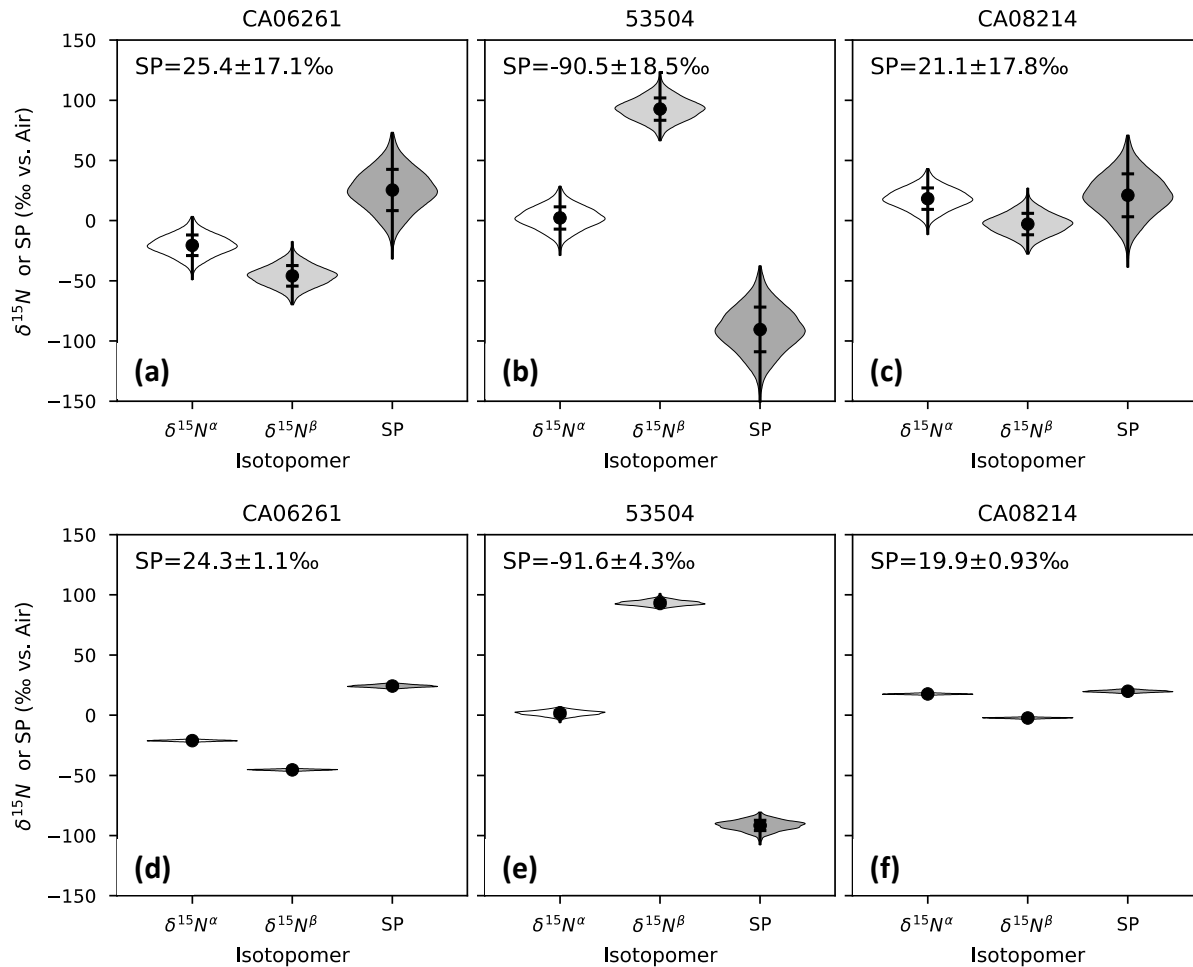
Figure 4. a-c) Isotopocule values and error associated with a 10 % relative uncertainty in γ – κ, based on Monte Carlo simulation results, for reference materials CA062621 (a), 53504 (b), and CA08214 (c). γ and κ were modeled as random numbers centered around γ = 0.174 and κ = 0.083, with the uncertainty in γ – κ equal to 10 % of the mean γ – κ (0.091). d-f) Isotopocule values and error associated with a 10% relative uncertainty in the absolute values of γ – κ, holding the difference γ – κ constant, for reference materials CA062621 (d), 53504 (e), and CA08214 (f). γ and κ were modeled in tandem as random numbers centered around γ = 0.174 and κ = 0.083, with uncertainties equal to 10% of the mean γ, and γ – κ was held constant at 0.091. Violin plots are based on a kernel density estimate of the distribution and the values plotted and reported on each figure show the mean value ±1σ.